HMG Advance Access published May 18, 2012

Inhibition of Tau aggregation in a novel *C. elegans* model of Tauopathy mitigates proteotoxicity

Chronis Fatouros[1,2,3,§], Ghulam Jeelani Pir[4,5,§], Jacek Biernat[4,5], Sandhya Padmanabhan Koushika[7], Eckhard Mandelkow[4,5,6], Eva-Maria Mandelkow[4,5,6], Enrico Schmidt[1,2,$,#], Ralf Baumeister[1,2,8,#,*]

[1] Faculty of Biology, Institute of Biology III, and Faculty of Medicine, Center for Biochemistry and Molecular Cell Research (ZBMZ), University of Freiburg, 79104 Freiburg, Germany

[2] Center for Biological Systems Analysis (ZBSA), 79104 Freiburg, Germany

[3] International Max Planck Research School for Molecular and Cell Biology (IMPRS-MCB)

[4] German Center for Neurodegenerative Diseases (DZNE), 53175 Bonn, Germany

[5] Max Planck Institute for Neurological Research (MPINF), 50931 Cologne, Germany

[6] CAESAR Research Center, 53175 Bonn, Germany

[7] Department of Biological Sciences, Tata Institute of Fundamental Research, Homi Bhabha Road, Mumbai 400 005, India

[8] Center for Biological Signalling Studies (BIOSS) and Freiburg Center for Advanced Studies (FRIAS), University of Freiburg, 79104 Freiburg, Germany

[§] contributed equally to this paper

[$] Current address: Center for Proteomic Chemistry, Novartis Pharma AG, Basel, Switzerland

[#] contributed equally

* Author for correspondence: Prof. Dr. Ralf Baumeister, Institute of Biology III, Schaenzlestrasse 1, D-79104 Freiburg, Tel. +49-761-203 8350, Fax +49-761-203 831, Email: baumeister@celegans.de

© The Author 2012. Published by Oxford University Press.
This is an Open Access article distributed under the terms of the Creative Commons Attribution Non-Commercial License (http://creativecommons.org/licenses/by-nc/3.0), which permits unrestricted non-commercial use, distribution, and reproduction in any medium, provided the original work is properly cited.

Downloaded from http://hmg.oxfordjournals.org/ at Universitaet Freiburg on March 21, 2013

Abstract

Increased Tau protein amyloidogenicity has been causatively implicated in several neurodegenerative diseases, collectively called Tauopathies. In pathological conditions, Tau becomes hyperphosphorylated and forms intracellular aggregates. The deletion of K280, which is a mutation that commonly appears in patients with Frontotemporal Dementia with Parkinsonism linked to chromosome 17, enhances Tau aggregation propensity (pro-aggregation). In contrast, introduction of the I277P and I308P mutations prevents β-sheet formation and subsequent aggregation (anti-aggregation). In this study, we created a Tauopathy model by expressing pro- or anti-aggregant Tau species in the nervous system of *C. elegans*. Animals expressing the highly amyloidogenic Tau species showed accelerated Tau aggregation and pathology manifested by severely impaired motility and evident neuronal dysfunction. In addition, we observed that the axonal transport of mitochondria was perturbed in these animals. Control animals expressing the anti-aggregant combination had rather mild phenotype. We subsequently tested several Tau aggregation inhibitor compounds and observed a mitigation of Tau proteotoxicity. In particular, a novel compound that crosses the blood brain barrier of mammals proved effective in ameliorating the motility as well as delaying the accumulation of neuronal defects. Our study establishes a new *C. elegans* model of Tau aggregation-mediated toxicity and supports the emerging notion that inhibiting the nucleation of Tau aggregation can be neuroprotective.

Downloaded from http://hmg.oxfordjournals.org/ at Universitaet Freiburg on March 21, 2013

Introduction

Aggregation of mutant or even wild type, hyperphosphorylated Tau is a common factor in the course of several neurodegenerative diseases collectively called Tauopathies (1-5). An unresolved debate in the field focuses on the role of terminal Tau aggregates termed Neurofibrillary Tangles (NFTs) for the pathogenesis of the disease. It is still unclear whether these are the cause of neuronal toxicity, or whether they result from an effort of the cell to sequester the more toxic oligomers that could disrupt various cellular functions, such as axonal transport (4, 6, 7). A deluge of recent evidence points to the pre-tangle oligomers with high propensity to aggregate as being the instigating factor of toxicity, not only for Tau [reviewed in (7)], but also for amyloid-beta or Huntingtin (8, 9). Their continuous presence in the cell is detrimental, while no correlation was detected between neuronal toxicity and the formation of tangles which can persist even after expression of transgenic Tau has been switched off (10-14).

An experimental approach to uncouple the aggregation-mediated toxicity of Tau from other functions involves the ΔK280 pro-aggregation mutation which is found in patients with FDTP-17 (15) and the respective anti-aggregation mutations I277P and I308P in the hexapeptide motifs. These substitutions prevent the formation of a beta sheet structure and thus hinder aggregation (10-13, 16). These studies have shown that the pro-aggregant Tau species is very toxic, while at a similar expression level the anti-aggregant species is not (16). Moreover, the F3ΔK280 fragment of Tau (aa 258-360) has been shown to act as a nucleation agent, and leads to accelerated toxicity by promoting the aggregation of both mutant and wild type Tau (17).

The *C. elegans* system presents numerous practical advantages, especially for high throughput screening approaches (18-21). As a result, transgenic strains expressing various human Tau mutations have been studied by several groups as disease models (22-27). However, a common theme in these previously published Tauopathy models is that they only develop a significant proteotoxicity phenotype at rather advanced age. Specifically, it has been shown that expression of hyperphosphorylated, mutated Tau protein, but also wild type Tau, can lead to progressive accumulation of structural damage such as axonal breaks in the GABAergic motor neurons and age-dependent defects in locomotion (25). Additionally, the expression of different Tau mutants (P301L

Downloaded from http://hmg.oxfordjournals.org/ at Universitaet Freiburg on March 21, 2013

and V337M) in the *C. elegans* nervous system was reported to result in Tau pathology (24). Kraemer *et al.* used their Tauopathy model to perform a mutagenesis screen, uncovering two new factors that participate in the pathological cascade, namely SUT-1 and SUT-2 (22, 26, 28). The latter was shown in a follow-up study to have a direct homologue in humans (MSUT-2), whose knock-down also alleviated Tau pathology in a mammalian cell culture model (28). These seminal contributions served as proof of principle, showing that human Tau mutants can indeed recapitulate neuron related phenotypes in the worm, and that insights gained in such a time and cost-effective model can have relevance for understanding the disease in humans. Importantly, studying human Tau mutants in *C. elegans* has the advantage of avoiding interference with endogenous Tau, since the only Tau homologue in the worm, PTL-1, is only expressed in a small subset of neurons (29, 30).

Here, we take advantage of the well documented molecular dissection of Tau aggregation-mediated toxicity (11, 13, 16) and establish a *C. elegans* model of Tauopathy based on the highly amyloidogenic ΔK280 Tau mutation. We strove to achieve a strong toxicity phenotype that could be attributed to the process of accelerated aggregation already in young adult worms. For this purpose, we introduced a pan-neuronally expressed pro-aggregant F3ΔK280 Tau fragment (encompassing the repeat domain of Tau) in the full length (FL) Tau V337M strain CK10 (22), using the anti-aggregant F3ΔK280-PP transgene as a control. Pro-aggregant Tau led to substantially increased toxicity in the worms. This recapitulated the main aspects of Tauopathy known from mammalian models of the disease (4, 6, 13), manifested by uncoordinated movement from the first day of adulthood, axonal defects such as gaps and varicosities in motor neurons, impaired pre-synaptic areas and perturbed axonal transport of mitochondria. The anti-aggregant combination caused only a mild phenotype with a significantly reduced level of morphological abnormalities. We also showed that the levels of rapidly aggregating Tau in the pro-aggregant worms are increased. Treating the worms with Methylene Blue (MB), an aggregation inhibitor of the phenothiazine class (31, 32) resulted in beneficial effects. We also demonstrated that treatment of the pro-aggregant transgenic strains with a novel Tau aggregation inhibitor, a compound belonging to the aminothienopyridazine (ATPZ) class [compound #16 in (33), hereafter referred to as cmp16], ameliorated the motility phenotype, reflected also by a reduced extent of the progressive accumulation of neuronal morphological abnormalities.

Downloaded from http://hmg.oxfordjournals.org/ at Universitaet Freiburg on March 21, 2013

Results

Rapid deposition of Tau aggregates in the nervous system of *C. elegans* led to early onset of uncoordinated phenotype.

Our first aim was to create a novel Tauopathy model in the nematode *C. elegans* that allows distinction of pathological mechanisms specifically induced by aggregation of the Tau protein. For this purpose we focused on the well characterized ΔK280 mutation (10-13) which specifically leads to aggregation-mediated toxicity. We generated transgenic strains expressing chromosomally integrated versions of the amyloidogenic F3ΔK280 fragment of human Tau [derived from the repeat domain of TauΔK280, (16, 17)] from the *rab-3* promoter, to achieve pan-neuronal expression. In one set of *C. elegans* strains we expressed the pathological FDTP-17 mutant ΔK280 which enhances aggregation whereas the other set harbors, in addition to ΔK280, the proline substitutions I277P and I308P (PP), which act as beta-sheet breakers and prevent aggregation (15). We obtained two independently integrated lines for each mutant which we then backcrossed to wild type N2 worms 10 times each, to get rid of possible background mutations caused by the insertion events. Our hypothesis was that the strains carrying integrated transgenes of the pro-aggregant F3ΔK280 (*byIs161*, *byIs193*) would result in a more pronounced phenotype than that of the strains expressing the anti-aggregant F3ΔK280-PP transgenes (*byIs162*, *byIs194*). However, the locomotion phenotype of day 1 adult animals of these single transgenic strains was very similar (Supplementary Material, Fig. S1A), which could be the consequence of the nucleation process being too slow compared to the short lifespan of the animals. We therefore crossed each of these strains with CK10, a previously characterized strain that expresses pan-neuronal FL Tau V337M (23, 24). We hypothesized that co-generating full length mutant Tau and the F3ΔK280 fragment should potentiate nucleation of aggregation and result in increased toxicity. Indeed, strongly defective locomotion phenotype developed at day 1 of adulthood for both strains expressing FL Tau plus F3ΔK280 (BR5485 pro-aggr. line 1 mean speed ± standard deviation = 70.6±17.9 µm/sec and BR5706 pro-aggr. line 2 speed=60.8±22.3 µm/sec), compared to both the anti-aggregant strains expressing FL Tau plus F3ΔK280-PP (BR5486, anti-aggr line 1, speed=103.5±29.5

Downloaded from http://hmg.oxfordjournals.org/ at Universitaet Freiburg on March 21, 2013

µm/sec and BR6427 anti-aggr line 2, speed=108.7±27.5 µm/sec; Fig. 1A). The latter strains did not exhibit obvious locomotion defects (Supplementary Material, Movies S1-S3).

We verified with Western blot analysis that the independently integrated transgene arrays are expressed at similar levels in both sets of strains (Fig. 1B and 1C). We also performed antibody staining to confirm that Tau is properly expressed in the nervous system (Fig. 1D-1F). Since the two independent strains for each transgene combination had similar phenotype and comparable expression levels, we decided to further analyze one strain from each set, namely the pro-aggregant line 1 (with the *byIs161* transgene) and the anti-aggregant line 1 (with the *byIs162* transgene).

In order to quantitate aggregate formation, we applied Thioflavin-S (ThS) staining which detects amyloid deposits (34, 35) on synchronous young adult populations of worms, including worms expressing just the transformation marker as control. We observed extensive ThS staining at the nerve ring of the pro-aggregant strain (mean number of aggregates = 14.6, range=1 to 64), while the anti-aggregant strain showed only minimal staining (mean=2.2, range 0 to 6), similar to negative controls (mean=0.7, range = 0 to 2). Representative images are shown in (Fig. 1G-1I) and quantification is shown in (Supplementary Material, Fig. S1B). We next extracted Tau aggregates from these worms using formic acid (FA) (Fig. 2A). The pro-aggregant F3ΔK280 fragment appeared only in the detergent insoluble fraction (FA fraction), whereas the anti-aggregant F3ΔK280-PP appeared solely in the soluble RAB fraction (Fig. 2A, upper panel), suggesting that the pro-aggregation construct indeed preferably aggregated. In addition, only FL Tau V337M was phosphorylated at the KXGS motif (Fig. 2A**,** mid panel, 12E8) and S396, S404 (PHF-1 epitope) (Fig. 2A**,** lower panel, PHF-1). We then extracted Tau from 7 day old worms and detected both detergent soluble and the insoluble aggregates even in the CK10 strain (FL Tau V337M) as reported earlier (24). However, the pro-aggregant strain displayed ~4 times more aggregated Tau (Fig. 2B). We conclude that F3ΔK280 fragment is capable of accelerating the aggregation of full-length Tau, and this process can be monitored in the short lifespan of *C. elegans*, causing an easily distinguishable phenotype.

Hyperphosphorylation of Tau is complex and has been suggested to play a role in its toxicity (36-39) even in the absence of higher-order aggregates (40, 41), while other studies have shown a dissociation of hyperphosphorylation and toxicity (42, 43). Therefore, we wanted to determine the

Downloaded from http://hmg.oxfordjournals.org/ at Universitaet Freiburg on March 21, 2013

phosphorylation status of the sequentially extracted Tau from our transgenic strains. Both the soluble and insoluble Tau from all three Tau transgenic strains were phosphorylated at various sites and the CP13, AT8 and AT100 epitopes revealed reduced phosphorylation in the CK10 strain compared to the pro-aggregant strain and least levels of phosphorylation in the anti-aggregant strain (Supplementary Material, Fig. S2). Overall, Tau both in the soluble and the insoluble fractions was phosphorylated to a higher degree in the pro-aggregant strain compared to the other two strains.

In order to add further support to our hypothesis that the locomotion defect phenotype that we described was caused by Tau aggregation-mediated toxicity and not by unknown neighborhood effects of the transgene insertion event, we performed RNAi against Tau after crossing the strains into a neuronal RNAi sensitizing mutant background [strain *eri-1(mg366)IV;lin-15B(n744)X* (44)]. The motility of the pro-aggregant worms was considerably enhanced upon applying RNAi against F3ΔK280 (speed=70.7±17 µm/sec for RNAi-treated versus 40.3±17 for control), while the anti-aggregant worms showed no difference upon treatment (Supplementary Material, Fig. S1C). In addition, introducing a non-integrated extrachromosomal array expressing F3ΔK280 also reduced motility of the FL Tau V337M strain (by ~30%), whereas a F3ΔK280-PP extrachromosomal array did not (Supplementary Material, Fig. S1D). These experiments suggested that the phenotypic differences observed are indeed due to the differential aggregation propensities of the Tau fragments and were not caused by transgene insertion. In summary, we conclude that expression of the highly amyloidogenic combination of Tau species leads to rapid formation of aggregates and overt toxicity in *C. elegans*, manifested by uncoordinated locomotion, whereas the anti-aggregant combination does not.

Accelerated aggregation of Tau caused morphological abnormalities in the motor neurons of *C. elegans.*

We next hypothesized that the locomotion phenotype is caused by damage in the motor neurons, since the transgenes are expressed in the whole nervous system and neuronal structural defects have been demonstrated in previous neurodegenerative *C. elegans* models (24, 25). We first looked at the GABAergic motor neurons, using the *juIs73*:[*Punc-25::gfp*]III reporter (45) and measured the number of axonal discontinuities (gaps) in the ventral and dorsal cords of the animals during larval stages as well as during adulthood (representative example of a wild type young adult animal is shown in Fig.

Downloaded from http://hmg.oxfordjournals.org/ at Universitaet Freiburg on March 21, 2013

3A). In wild type animals, the development of the nervous system is mostly completed in the L3 stage. Correspondingly, GFP stained processes show no gaps and have continuous dorsal and ventral cords (Fig. 3D). In contrast, we observed severe developmental defects in the pro-aggregant strain (BR5707), that manifest as increased numbers of persistent gaps both in the ventral and dorsal neural cords (mean±s.d= 2.7±1.4 gaps at the L3 stage). Gaps were still visible at the L4 stage (Fig. 3D). At day 1 of adulthood we observed 1.32±0.8 gaps in the cords of the pro-aggregant strain (example of a young adult in Fig. 3C). In contrast, the anti-aggregant strain (BR5674) did not show comparable morphological defects during development (Fig. 3D) and as young adults (example in Fig. 3B) they showed very few, if any, gaps (mean±s.d.=0.13±0.3). The number of axonal gaps in the pro-aggregant strain rose with age, so that by day 5 of adulthood almost 100% of the worms showed axonal gaps (3.1±0.9) (Fig. 3D). By that age the anti-aggregant strain showed a reduced number of gaps (1.1±0.9) which was not very different from wild type (0.5±0.4) (Fig. 3D). To corroborate this result, we also looked at the cholinergic motor neurons, which provide the activating signals to the neuromuscular junctions in coordination with the GABAergic inhibitory neurons on the opposite side (46). For this purpose, we introduced an extrachromosomal array to mark the cholinergic neurons [*Punc-129::mCherry*] and examined the ventral and dorsal cords of young adult animals for morphological abnormalities. The wild type reporter strain (BR6061) and the anti-aggregant strain (BR6089) showed rare occurrence of gaps (wt: 2.3±0.5 % animals with gaps, 8.5±3.2 % in anti-aggregant) (Fig. 3E and Supplementary Material, Fig. S3). In contrast, the pro-aggregant strain showed frequent occurrence of gaps (27.8±4.8 % of day 1 adult animals), similar to those observed in the GABAergic neurons (Fig. 3E and Supplementary Material, Fig. S3). From this data we conclude that the continued expression of FL Tau V337M and F3ΔK280 is toxic for the neurons and as a consequence, the development of the nervous system is perturbed. The continuous rise of the number of gaps later in adulthood suggests that progressive axonal degeneration follows the initial developmental defects. Combination of FL Tau V337M with the non-amyloidogenic F3ΔK280-PP produced only mild defects which only in day 5 old animals became statistically distinguishable from wild type.

Downloaded from http://hmg.oxfordjournals.org/ at Universitaet Freiburg on March 21, 2013

The pro-aggregant strain had defective accumulation of Synaptobrevin-1 in the pre-synaptic termini indicating impaired presynaptic transmission.

Aberrant phosphorylation and aggregation of Tau have been linked to axonal transport problems, synaptic malfunction and degeneration (6). In order to examine synapse morphology in Tau expressing worms, we used as a marker the reporter gene *nIs52*:[*Punc-47::snb-1::gfp*] (47) that expresses GFP fused to Synaptobrevin-1 from the motor neuron-specific *unc-47* promoter. For quantitation, we focused on analyzing the dorsal neural cord at the posterior gonadal arm (Fig. 4A - 4C). In the wild type strain, SNB-1::GFP formed a regular pattern of puncta along the neural cord (Fig. 4D) as described before (48). This pattern was similar to that of the anti-aggregant strain (BR5793, Fig. 4E). In contrast, the pro-aggregant strain (BR5792) displayed a discontinuous punctate pattern and staining was generally more diffuse in pre-synaptic areas, which we take as an indicator for synaptic transport defects or potentially synaptic loss (Fig. 4F). In older animals, this phenotypic pattern deteriorated further (Supplementary Material, Fig. S4A-S4F). We quantitated the mean of the fluorescence intensity in SNB-1::GFP puncta from 25 animals of each genotype (Fig. 4G-4I) and found that the puncta intensity of the pro-aggregant strain was reduced (mean intensity±s.d.=1022±330 arbitrary units, AU) compared to both wild type (1410±300 AU) and anti-aggregant (1292±400 AU) strains (Fig. 4J). Moreover, the density of puncta (number of puncta per 50 µm) was also reduced (Fig. 4K). Specifically, pro-aggregant worms had 8.9±5.1 puncta per 50 µm, whereas wild type had 14.1±3.3 and the anti-aggregants had 12.5±3.5. This indicated that SNB-1 failed to properly accumulate at the presynaptic termini of young adult pro-aggregant worms. At day 5 of adulthood, reduction of puncta numbers was already seen in wild type and anti-aggregant strains compared to young adults. However, the staining loss was more pronounced for the pro-aggregant strain (Supplementary Material, Fig. S4J). Since previous experiments performed by others (48, 49) suggested a correlation of SNB-1 puncta with the presence of synapses, we are confident that our marker staining faithfully represents the alterations of presynaptic structures.

This finding suggests that synaptic transmission may be negatively affected. In order to test neurotransmission in the individual strains, we performed aldicarb and levamisole sensitivity assays with day 1 adult animals (50). Worms with functional neurotransmitter release should be sensitive to

Downloaded from http://hmg.oxfordjournals.org/ at Universitaet Freiburg on March 21, 2013

both substances and become paralyzed due to muscle hypercontraction (50). Resistance to aldicarb can arise from either a pre- or a post-synaptic perturbation, while resistance to levamisole typically indicates a post-synaptic defect (50). Animals of the pro-aggregant strain displayed a mild resistance to aldicarb, producing a paralysis profile intermediate between the sensitive wild type N2 and the resistant *rab-3(js49)* strain which we used as controls (Fig. 5A). The anti-aggregant strain also displayed mild resistance to aldicarb, although animals typically became paralyzed earlier than pro-aggregants (Fig. 5A the small difference between anti-aggregant and pro-aggregant strains was not statistically significant). All the transgenic strains were sensitive to levamisole and indistinguishable from wild type (Fig. 5B). Taken together, these experiments suggest both anti- and pro-aggregant strains may display pre-synaptic defects. This corresponds to the observed SNB-1 puncta defect at the pre-synaptic termini of the pro-aggregant strain. We conclude that expression of amyloidogenic Tau fragments in combination with FL Tau V337M perturbs proper presynaptic organization in this *C. elegans* Tauopathy model.

The pro-aggregant Tau strain showed mislocalized mitochondria in the DA9 motor neuron

Mitochondrial transport problems have been suggested to contribute to the progression of pathology in most mammalian neurodegeneration models, so we examined whether our Tauopathy model recapitulates the neuronal mitochondria mislocalization phenotype (6, 51-53). For this purpose, we took advantage of the *wyEx2709* [*Pitr-1::TOM-20*$^{1\text{-}54aa}$*::yfp*] reporter strain (54), which labels mitochondria only in the DA9 neuron close to the posterior end of the animal. The soma of the DA9 neuron is located at the ventral side near the anus, and extends a dendrite anterioventrally, and an axon towards the dorsal cord which then extends anteriodorsally. This region typically displays a regular distribution of mitochondrial particles (54) (Fig. 6A), extending to the distal axonal segment. The vertical axonal part is asynaptic and has few mitochondria (54). We crossed *WyEx2709* into the pro-aggregant strain (resulting in strain BR6011), and discovered that this regular mitochondrial distribution was distorted. Few or no mitochondrial particles were detected in the distal axonal segment (example in Fig. 6C) whereas the anti-aggregant strain (BR6012) showed only a moderate perturbation (example in Fig. 6B). Almost 60% of the axonal mitochondria accumulated in the proximal region and typically did not reach the more distal parts of the axon in the animals of the pro-

Downloaded from http://hmg.oxfordjournals.org/ at Universitaet Freiburg on March 21, 2013

aggregant strain. In contrast, only 32% and 45% of the axonal mitochondrial population was localized to the proximal axonal segment of wild type and anti-aggregant strain, respectively (Fig. 6D and Supplementary Material, Fig. S5). It is unclear whether this mislocalization arose from a severe transport problem or from axonal retraction, reminiscent of the axonal gaps in (Fig. 3). In summary, the results shown so far further support the notion that a highly amyloidogenic Tau species is detrimental for neurons, whereas the non-amyloidogenic species does not cause severe problems.

Axonal transport was perturbed in mechanosensory neurons of the pro-aggregant, but not the anti-aggregant Tau transgenic worms.

We reasoned that aggregation-prone Tau species might affect axonal transport properties which, for example, may alter the motility of mitochondria. The strain *jsIs609* expresses GFP with a mitochondrial localization signal (MLS) in the six mechanosensory neurons of *C. elegans*. We crossed this strain with our Tau mutants, creating the pro-aggregant (BR6174) and the anti-aggregant (BR6175) mitochondrial marker strains. To quantify mitochondrial movements, we performed single plane live imaging of the middle axonal segment of the PLML or PLMR neurons in immobilized worms, for about 8 to 10 minutes per time lapse (see Materials & Methods). For analysis we selected in each animal the PLM axon closer to the microscope objective. We chose these posterior neurons for two reasons: a) because analysis of the axons of the other mechanosensory neurons is frequently obscured by gut autofluorescence or the GFP transformation markers used, and b) our immobilization protocol, which does not use anesthetics, results in animals that can still slightly move their heads and have a pumping pharynx, both may affect the quality of data acquisitions. We collected time lapse acquisitions from 20 animals of each strain, representative examples of which are shown as kymographs in (Fig. 7A-7C) and as movies in the Supplementary Material (Movies S4-S6). We manually tracked each moving GFP particle with ImageJ and extracted the instantaneous velocity values of continuously moving particles (Fig. 7D). The velocity of mitochondrial transport in the pro-aggregant strain was lower than in wild type (mean±s.d.=171±111 nm/sec versus 256±117 nm/sec), whereas the anti-aggregant strain (194±131 nm/sec) did not substantially differ from wild type (Fig. 7D). In addition, a striking difference in the mitochondrial pausing frequency was observed between pro-aggregant and the other two strains, with approximately four times more frequent pause events for

Downloaded from http://hmg.oxfordjournals.org/ at Universitaet Freiburg on March 21, 2013

the pro- compared to the anti-aggregant (Fig. 7E). This suggests that mitochondrial transport in the axons of this strain is perturbed. The mitochondrial flux (number of moving mitochondria per minute) was slightly reduced in both Tau transgenics (Fig. 7F), and the ratio of mobile to stationary mitochondria was also lower, particularly in the pro-aggregants (Fig. 7F), although these differences proved to be not statistically significant. The range of track lengths we recorded for the pro-aggregants was from 1 to 33.1 µm (mean=6.31 µm), while for the anti-aggregants we recorded a range from 1.6 µm to 87.2 µm (mean=14.39 µm) and for the wild type these values ranged from 2.7 µm to 87.3 µm (mean=19.2 µm) (Fig. 7G). Taken together, the track length of mitochondria in a given time lapse was smaller in the pro-aggregant strain. In summary, we found that several phenotypic criteria tested allow us to distinguish between pro-aggregant and anti-aggregant Tau transgenic strains. Therefore, our *C. elegans* model indicates that amyloidogenic properties of Tau block axonal transport of mitochondria.

A novel Tau aggregation inhibitor compound ameliorated the phenotype of the pro-aggregant strains and mitigated neurotoxicity.

The pathology we observed in *C. elegans* is reminiscent of the cellular pathology observed in mammalian Tauopathy models. Aiming to see whether we can ameliorate the phenotype, we set out to test small molecule compounds that have already been shown to have Tau anti-aggregation properties *in vitro*. As a proof of principle, we first tested the efficacy of Methylene Blue (MB), a Tau aggregation inhibitor with potential cognition-enhancing effects (55, 56). We supplemented the growth medium of synchronized L1 larvae (pro-aggregant strain) with 25 µM Methylene Blue and measured their locomotion speed as day 1 young adults. This treatment led to 15% amelioration of locomotion (Supplementary Material, Fig. S6A). Higher MB concentrations were not effective. At the biochemical level, MB treatment altered Tau solubility, shifting the equilibrium towards more soluble Tau and reduced detergent insoluble Tau by ~35% in the pro-aggregant strain (Fig. 8A, quantitation in 8B), consistent with its anti-aggregation properties (31). We then applied, in 96-well liquid culture format, the two most promising hit compounds obtained in a mammalian cell model of Tau toxicity (57), namely the phenylthiazolyl-hydrazide derivatives Bsc3094 and bb14, and observed a similar amelioration effect in locomotion (Fig. S6B). BSc3094 resulted in 40% decrease in the detergent

Downloaded from http://hmg.oxfordjournals.org/ at Universitaet Freiburg on March 21, 2013

insoluble Tau (FA fraction) in pro-aggregant animals, but there was no apparent change in the detergent insoluble monomeric Tau after bb14 treatment (Fig. 8C, quantitation in 8D).

The successful treatment using a small molecule served as a proof of principle suggesting that the *C. elegans* Tauopathy model we generated is well suited for the *in vivo* testing of compounds in high throughput. We next analyzed the most prominent Tau aggregation inhibitor compound from a recently published *in vitro* screen [compound #16 in (33)], which belongs to the aminothienopyridazine (ATPZ) class of Tau inhibitors (5-Amino-3-(4-chlorophenyl)-N-cyclopropyl-4-oxo-3,4-dihydrothieno[3,4–d]pyridazine-1-carboxamide, referred to as cmp16 for simplicity, structure shown in Fig. 9A). This compound prevents Tau fibril formation *in vitro*, and is able to cross the mammalian blood-brain-barrier, an attribute that makes it favorable for clinical applications (33). We incubated pro-aggregant L1 larvae with increasing concentrations of cmp16 until adulthood. At 100 µM we observed improved locomotion of treated animals. These animals moved ~1.6 times faster than DMSO-treated controls (Fig. 9A). The compound did not have an effect on the other strains tested, suggesting that it acts specifically by reducing the toxicity of the amyloidogenic F3ΔK280 fragment (Supplementary Material, Fig. S6C). To visualize whether cmp16 is successful in reducing neural outgrowth defects, we also treated the pro-aggregant GABAergic reporter strain (described in Fig. 3) using the same conditions. For this purpose, we sampled animals at day 1, day 3 and day 5 of adulthood, and counted the number of axonal discontinuities in the motor neurons. Treatment with cmp16 diminished the progressive accumulation of neurite gaps in the motor neurons of the pro-aggregant animals compared to the DMSO treated controls (from 3.2±1 gaps at day 5 of the DMSO-treated to 2.4±1 gaps of the cmp16-treated strains, $p<0.05$) (Fig. 9B). Lower accumulation of structural damage in neurons can be interpreted as a sign of reduced neurodegeneration (22, 58). This phenotype correlated with a reduction of the insoluble Tau species by ~50% in animals following cmp16 treatment (Fig. 8B, 8D). In summary, this data indicates that this novel Tau anti-aggregation compound may be neuroprotective.

Downloaded from http://hmg.oxfordjournals.org/ at Universitaet Freiburg on March 21, 2013

Discussion

In this study we created and characterized a new Tauopathy model in *C. elegans* by combining the expression of FL Tau V337M (Kraemer and Schellenberg 2007) and the F3 fragment harboring the FDTP-17 mutation ΔK280 (15). This model differs from previously described Tauopathy models in *C. elegans* (24, 25) since it is based on a well characterized pathology basis and shows a robust toxicity phenotype. The latter appears already at day 1 of adulthood, which allows the uncoupling from age-related alterations of proteostasis (59-62). Importantly, using this model allowed us to focus on Tau aggregation-mediated toxicity and decouple this effect from Tau hyperphosphorylation or association with microtubules or membranes. To achieve this, we did not restrict ourselves to comparing phenotypes of transgenic versus non-transgenic animals, as was done in previous *C. elegans* Tau studies. Instead, we compared strains both harboring FL Tau V337M, coexpressed either with a pro-aggregant F3ΔK280 or an anti-aggregant F3ΔK280-PP fragment. These strains revealed significant phenotypic differences that will allow using them for modifier screening assays. These F3 fragments have been shown to differ only in their amyloidogenic propensity and not in other aspects, such as microtubule interaction (both have very poor binding) or phosphorylation patterns (both contain only the few phosphorylation sites in the repeat domain) (12, 16). Consequently, this provides support that the toxicity which manifests itself through neuronal morphological abnormalities, loss of SNB-1 puncta and impaired mitochondrial transport correlates with the amyloidogenic potential of Tau moieties and this is in accordance with recent reports in mouse models (13).

Axonal transport of mitochondria is a vital process for neuronal physiology and it is not surprising that its perturbation is thought to contribute to the neurodegenerative demise (52, 63-66). We probed axonal transport of mitochondria in our system with two approaches. First we examined the localization of mitochondria along the axon of the DA9 tail neuron and found that there are proportionally less fluorescent puncta corresponding to tagged mitochondria in the distal axonal segment of the pro-aggregant strain. These mitochondrial accumulations that correspond to synapses made *en passant* along the DA9 neuron (54), suggest either a lack of supply of mitochondria to the most distal synapses, or they may be caused by a loss of synapses or axonal retraction. With the marker we used here we cannot distinguish between these possibilities, as we would need the co-

Downloaded from http://hmg.oxfordjournals.org/ at Universitaet Freiburg on March 21, 2013

expression of a soluble fluorescent protein to fill the axonal cytoplasm and discern its boundaries. However, the results obtained with the second method, time lapse imaging and tracking of moving mitochondria, support the interpretation that their transport is perturbed by the amyloidogenic Tau species. Although the instantaneous particle velocities are similar, the pausing frequencies in the pro-aggregation animals show a significant increase. This is reminiscent of the differences between fast and slow axonal transport in mammalian neurons, which differ not by the motor-driven instantaneous speed, but by the intervening pauses (67). Many mitochondrial particles in these animals demonstrate a characteristic motion of short bursts of displacement followed by pauses, reminiscent of a traffic jam (68). We conclude that such a mitochondrial behavior is unfavorable for the high energy demands of neurons.

The rapid occurrence of the neural toxicity phenotype already during development, but also its age-dependent progression supports the notion that the accelerated formation of amyloidogenic oligomers within neurons is the causative toxicity factor. The robust locomotion defect that appears in our transgenic model makes this aspect a particularly suitable read-out for time- and cost-effective pharmacological or genetic screens to uncover specific modulators of Tau pathology. Several other neurodegeneration screens have been successfully performed before in *C. elegans*, as exemplified for Tau (22), amyloid-beta peptide (69, 70), Huntingtin/polyQ (19, 71), and Spinal Muscular Atrophy (72) disease models. To demonstrate the value of our new model, we tested several compounds for which an efficacy against Tau aggregation has been suggested. These were Methylene Blue, which was already tested in mouse models (56, 73), BSc3094 and bb14 which demonstrated protective effects in cell culture models (57, 74, 75), and the ATPZ Tau inhibitor cmp16 which blocked Tau aggregation *in vitro* and has been shown to readily cross the blood-brain barrier of mice (33). We showed here that they are all capable of at least partially preventing or delaying Tau mediated toxicity in *C. elegans*. At the biochemical level we demonstrated a reduction of insoluble Tau after applying the compounds in liquid cultures. Concerning the bioavailability of the reported compounds, all of them have chemical structures such as benzene rings that have been found enriched in molecules that can accumulate within *C. elegans* tissues (76). This lends support to our interpretation that these compounds reach the neurons of the worms and act on Tau species inhibiting their aggregation.

Downloaded from http://hmg.oxfordjournals.org/ at Universitaet Freiburg on March 21, 2013

An important conclusion from this study is that, by inhibiting the aggregation process, neuronal damage can be thwarted. This we achieved in two ways: By expressing the F3Δ280-PP fragment, which does not allow accelerated aggregate formation, and by treating with compounds that have anti-aggregation capacities. This treatment is essentially effective if administered from the early larval stages onward, to suppress even the initial formation of toxic oligomers. Actively preventing the aggregation process is a promising therapeutic avenue and encompasses a particularly active research field (75, 77-80). Capitalizing on advances in structural and computational biology, non-natural amino acid inhibitors of Tau and polyQ aggregation have been recently developed (81, 82). Moreover, the compound Thioflavin-T which is predominantly known as a staining reagent for aggregates has been recently revisited and demonstrated to prevent widespread aggregation and proteotoxicity in worms (83). The fact that amyloidogenic intermediates share common structure (84), implies that compounds that are able to block the process in a non-protein-specific way can be effective in a wider range of protein folding disorders. In this study, we used MB, BSc3094 and bb14 as proof of principle, and demonstrated that a new compound belonging to the ATPZ class can be protective against Tau aggregation-mediated toxicity. It would be interesting to know whether this compound has therapeutic potential by testing it in mouse models of Tauopathies and, if proven effective, to promote it for clinical testing in an effort to curb the progression of this debilitating condition. Finally, this new *C. elegans* model of Tauopathy can be exploited for high-throughput screening approaches to uncover novel modulators of neurodegeneration.

Materials & Methods

Generation and maintenance of *C. elegans* strains

The following transgenic *C. elegans* strains were generated for this study: BR5270:*byIs161*[*Prab-3::F3ΔK280;Pmyo-2::mCherry*], BR5271:*byIs162*;[*Prab-3::F3ΔK280(I277P)(I308P);Pmyo-2::mCherry*], BR5944: *byIs193*[*Prab-3::F3ΔK280;Pmyo-2::mCherry*], BR6516: *byIs194*;[*Prab-3::F3ΔK280(I277P)(I308P);Pmyo-2::mCherry*], CK10: *bkIs10*[*Paex-3::h4R1NTauV337M;Pmyo-2::gfp*] was provided by Brian Kraemer (24), BR5485:*byIs161;bkIs10 (pro-aggregant line 1)*,

Downloaded from http://hmg.oxfordjournals.org/ at Universitaet Freiburg on March 21, 2013

BR5486:*byIs162*;*bkIs10* (anti-aggregant line 1), BR5706: *byIs193;bkIs10* (pro-aggregant line 2), BR6427: *byIs194;bkIs10* (anti-aggregant line 2), BR5625:*eri-1(mg366)IV;lin-15B(n744)X*;*byIs161;bkIs10* (Pro-aggregant, neuronal RNAi sensitized strain), BR5578:*eri-1(mg366)IV;lin-15B(n744)X*;*byIs162*;*bkIs10* (Anti-aggregant, neuronal RNAi sensitized strain), *juIs73*:[*Punc-25::gfp*]III provided by Erik Lundquist (45), BR5674:*byIs162;bkIs10;juIs73*, BR5707:*byIs161;bkIs10;juIs73*, *nIs52*:[*Punc-47::snb-1::gfp*] provided by Erik Jorgensen (47), BR5792:*byIs161*;*bkIs10;nIs52*, BR5793:*byIs162*;*bkIs10;nIs52*, BR5960:*bkIs10*;*Ex1069*[*Pmyo-2::mCherry;Prab-3::F3ΔK280*], BR5961:*bkIs10*;*Ex1070*[*Pmyo-2::mCherry;Prab-3::F3ΔK280(I277P)(I308P)*], *wyEx2709*:[*Pitr-1::TOM-20*$^{1-54aa}$*::yfp;Podr-1::gfp*], provided by Kang Shen (54), BR6011:*byIs161;bkIs10;wyEx2709*, BR6012:*byIs162;bkIs10;wyEx2709*, BR6088:*byIs161;bkIs10*;*Ex*[*Punc-129::mCherry*], BR6089:*byIs162;bkIs10*;*Ex*[*Punc-129::mCherry*], BR6061:*Ex*[*Prab-3::GFP*;*Punc-129::mCherry*], provided by Stefan Eimer, *jsIs609*:Is[*Pmec-4::MLS::gfp*] , BR6174:*byIs161;bkIs10;jsIs609*, BR6175:*byIs162;bkIs10;jsIs609*.

The following mutant strains were used in this study: BR4338: *eri-1(mg366)IV;lin-15B(n744)X* [sensitized strain for neuronal RNAi (44)], BR794: *lev-1(x21)IV*, NM791: *rab-3(js49)II*, (as resistant controls for the aldicarb and levamisole assays).

General worm handling and generation of transgenic worms was performed according to standard procedures described previously (85). Worm cultures were maintained at 20°C unless otherwise mentioned. Integration of extra chromosomal arrays was achieved after subjecting L4 transgenic larvae to 30 Gray dosage of γ-irradiation and screening the F2 generation for clones that have 100% fluorescent marker penetrance. The stable lines obtained were subsequently backcrossed to laboratory N2 wild type males for 10 rounds, to get rid of background mutations. The strains were typically thawed fresh from -80°C glycerol stocks every 4-5 months, to avoid (epi)genetic drift.

Sequential extraction of proteins

Synchronized worms were washed off NGM plates with M9 buffer. Dead animals and bacteria were removed by flotation on a 30% sucrose solution. The entire extraction procedure was carried out on ice and centrifugation steps were at 4°C except for the last step with 70% formic acid which was performed at room temperature. To extract the different Tau fractions (86), worm pellets after sucrose

Downloaded from http://hmg.oxfordjournals.org/ at Universitaet Freiburg on March 21, 2013

separation were directly resuspended in an equal amount (w/v) of high salt RAB buffer (100 mM 2-(*N*-morpholino) ethanesulfonic acid (MES), 1 mM EGTA, 0.5 mM MgSO4, 20 mM NaF). Worms were lysed by sonication (6 x10s, 10s break) on ice, and homogenates were centrifuged at 40,000 x g for 40 min. The supernatant constitutes the RAB fraction. The pellet was re-extracted with 1 M sucrose in RAB buffer and centrifuged 20 min at 40,000 x g, and the supernatant was discarded. The pellet was extracted with RIPA buffer (150 mM NaCl, 1% Nonidet P-40, 0.5% deoxycholate, 0.1% SDS, 50 mM Tris, pH 8.0) and centrifuged at 40,000 x g for 20 min. The supernatant is the RIPA fraction. The pellet after a brief washing with RIPA buffer was extracted with 70% formic acid (FA) and centrifuged at 13,000 x g for 15 min. The supernatant is the FA fraction. All buffers contained Complete Protease Inhibitor mixture 3x (Sigma-Aldrich P8340, Hamburg, Germany) and 0.5 mM PMSF.

Immunohistochemistry

Antibody staining was done as described previously (87). To detect Tau and F3 fragment together, the K9JA antibody was used at 1:20.000 dilution. An Alexa 488 goat anti-rabbit Antibody (1:5.000) was used for detection. Imaging was performed with a a Nikon A1 CLEM confocal through a Plan Apo VC 60x Oil DIC N2 objective using 14 % 488 laser power and 120 PMT value.

Thioflavin-S staining

Thioflavin-S (Sigma-Aldrich, Hamburg, Germany) was used to stain aggregates as described previously (34, 35), with the modification that the fixation procedure was performed according to the antibody-staining protocol to increase permeability of the cuticle. ThS signal was visualized with a Plan Apo VC 60x Oil DIC N2 objective and a 488 nm laser at 25% power, 110 PMT. Z-stacks were acquired with 1.5x zoom, and the region between the first and the second pharyngeal bulb (where the nerve ring is located) was examined for presence of ThS positive staining. For quantification, the acquired images were thresholded at 600 arbitrary intensity units, and spots were counted using the NIS Elements 3.0 software (Nikon).

Downloaded from http://hmg.oxfordjournals.org/ at Universitaet Freiburg on March 21, 2013

Live imaging

Images were acquired with a Nikon A1 CLEM confocal and a Nikon A1 CCD camera. Within each group of reporter strains the laser power and PMT values were kept constant, always avoiding oversaturation. For immobilizing the animals on the slides, a suspension of 1 % (v/v) solution of 0.1 µm diameter polystyrene beads (Polysciences Europe, Eppelheim, Germany) was used without the need for anaesthetics as described in (88). The worms become immobilized due to their inability to surpass friction between the beads and the underlying 8% agarose pad. Z-stacks of the posterior dorsal neural cord of *Punc-47::snb-1::gfp* reporter strains were collected with 30% GFP laser power, 150 PMT with a Plan Apo VC 60x WI DIC N2 objective and 2x zoom factor. Imaging of the DA9 tail neuron to visualize the mitochondrial marker *Pitr-1:TOM-20*$^{1\text{-}54aa}$*::yfp*, was performed with 30% power of a 514.5 nm laser, 140 PMT and 1,68 zoom factor of a Plan Apo VC 60x WI DIC N2 objective. For time lapse imaging of the *Pmec-4:MLS:gfp* mitochondrial marker, a 488 laser at 13,5% power and PMT=140 was used, , with 1.5x zoom factor of a Plan Apo VC 60x WI DIC N2 objective and 1,3 Airy units pinhole size. For each time lapse video, an axonal region of the PLML or PLMR neuron was selected that could be observed in a single plane, and 1 frame was acquired every 2 seconds, for 8 to 10 minutes.

Quantitation of synapses

In all sampled animals, the dorsal cord segment above the posterior gonadal arm was imaged and Z-stacks were acquired for comparisons. The resulting files were analyzed with NIS Elements 3.0 software (Nikon). A Region of Interest (ROI) was drawn around the neural cord, and a threshold was set at 600 intensity units, as well as at 0.5 µm diameter to select fluorescent puncta. Then the puncta number and the mean intensity for each punctum were calculated. The length of each imaged cord was measured as well, in order to extract the ratio number of synapses per 50 µm. For the compilation of the cumulative panels in (Fig. 4) and (Fig. S4), the ImageJ “Straighten” function was applied to straighten the cords, using line width of 50 pixels, and then the “Threshold” function was implemented, selecting the default B&W method and threshold level at 600 arbitrary intensity units.

Downloaded from http://hmg.oxfordjournals.org/ at Universitaet Freiburg on March 21, 2013

Aldicarb and Levamisole assays

We performed the aldicarb and levamisole assays as previously described (50, 89), using plates with 1 mM aldicarb (Supelco Germany Gmbh), and 0.2 mM levamisole (Fluka Analytical, Germany) respectively. The scoring of animals for paralysis was performed blind to the genotype with 30 animals per strains and the experiment was repeated 3 times.

Compound treatment

The compounds were applied in liquid culture in 96-well plate format. OP50 bacteria were grown overnight at 37°C in LB medium, collected by centrifugation, frozen at -80°C, and then resuspended in nematode S-medium (90), so that the OD_{595} was 1.5 in 4 times diluted samples. 20µl of this suspension were added per well. Synchronized L1 larvae were resuspended in S-medium supplemented with 10 µg/ml fungizone and 10 µg/ml cholesterol (both from Sigma-Aldrich) in an appropriate volume so that there is approximately 1 worm per µl and 20 µl were added per well. Finally, 40 µl of a 2X compound solution in S-medium was added per well, reaching a total volume of 80 µl. The final concentrations used in the experiments were 100µM cmp16, 50 µM BSc3094, and 50 µM bb14 each in 1% DMSO. Worms cultured in 1% DMSO served as treatment control. Water soluble Methylene Blue was used at a final concentration of 25 µM, with H_2O as control. Plates were sealed with parafilm and incubated at 20°C for 4 days. The worms were then transferred to empty NGM plates to measure the locomotion speed by acquiring and analyzing movies as described in the Supplementary Methods. For the biochemical characterization, the same procedure was scaled up for 6-well plate format, having 5 ml final volume added per well. Synchronized L1 larvae were added to the wells containing the compounds of interest and when the worms became L4 larvae, 75µM FuDR was added to prevent spawning of progeny. The worms were allowed to grow at 20°C with constant shaking until harvested for the protein extraction.

Statistical analysis

For statistical analyses the software Graphpad Prism 4.03 was used (GraphPad Software Inc., LaJolla, CA, USA). One-way ANOVA was used for comparisons between three or more groups with Tukey post-hoc test for comparisons between all groups. In case of non-parametric distributions, Kruskall-

Downloaded from http://hmg.oxfordjournals.org/ at Universitaet Freiburg on March 21, 2013

Wallis ANOVA with Dunn's post-hoc test was used instead. For the time course experiments with the drug treatments, two-way ANOVA with Bonferroni correction was applied. For the comparison of mitochondrial distributions the Yates' Chi Square test was used. In all graphs, the error bars depict the Standard Deviation (s.d.), unless otherwise mentioned. Differences at $p<0.05$ were accepted as statistically significant.

Supplementary data

Supplementary data and movies related to this paper are available at *Human Molecular Genetics* online (http://hmg.oxfordjournals.org)

Downloaded from http://hmg.oxfordjournals.org/ at Universitaet Freiburg on March 21, 2013

Author contributions

CF created the transgenic strains that were used in this study (excluding *jsIs609* and the ones provided by others as defined in the Methods), performed all the imaging and phenotypic characterization experiments and co-wrote the paper. GJP performed the cloning and all the biochemical experiments and contributed the relevant parts of the Materials & Methods and Results sections. SPK created the *jsIs609* strain in Michael L. Nonet's laboratory. EM, EMM, ES and RB proposed and supervised the study, co-wrote the paper and received the financial means to accomplish it.

Acknowledgements

We are grateful to the following people for providing strains and reagents crucial for this study: Brian Kraemer, Yishi Jin, Stefan Eimer, Kang Shen, Erik Lundquist, Erik Jorgensen and Peter Davies. Senexis Limited (Babraham Research Campus, Cambridge, UK) kindly provided the Tau inhibitor compound 16 (cmp16). E.M., E.M.M. and R.B. were supported by MEMOSAD, a Collaborative Project receiving funds from the European Community's Seventh Framework Programme (FP7/2007-2011 under Grant Agreement No. 200611). Additional support was provided by BIOSS and FRIAS (The German Excellence Initiative) to R.B. and Metlife Foundation (to E.M. and E.M.M.). We also thank Malikmohamed Yousuf and Ursula Schäffer for helpful discussions and comments.

Conflict of interest

The authors declare no conflicts of interest.

Downloaded from http://hmg.oxfordjournals.org/ at Universitaet Freiburg on March 21, 2013

References

1. Ballatore C., Lee V. M.-Y. and Trojanowski J. Q. (2007) Tau-mediated neurodegeneration in Alzheimer's disease and related disorders. *Nat. Rev. Neurosci.*, **8**, 663-672.

2. Congdon E. E. and Duff K. E. (2008) Is tau aggregation toxic or protective? *J. Alzheimers. Dis.*, **14**, 453-457.

3. Iqbal K., Wang X., Blanchard J., Liu F., Gong C.-X. and Grundke-Iqbal I. (2010) Alzheimer's disease neurofibrillary degeneration: pivotal and multifactorial. *Biochem. Soc. Trans.*, **38**, 962-966.

4. Obulesu M., Venu R. and Somashekhar R. (2011) Tau mediated neurodegeneration: an insight into Alzheimer's disease pathology. *Neurochem. Res.*, **36**, 1329-1335.

5. Reiniger L., Lukic A., Linehan J., Rudge P., Collinge J., Mead S. and Brandner S. (2011) Tau, prions and Abeta: the triad of neurodegeneration. *Acta Neuropathol.*, **121**, 5-20.

6. Morris M., Maeda S., Vossel K. and Mucke L. (2011) The Many Faces of Tau. *Neuron*, **70**, 410-426.

7. Spires-Jones T. L., Kopeikina K. J., Koffie R. M., de Calignon A. and Hyman B. T. (2011) Are tangles as toxic as they look? *J. Mol. Neurosci.*, **45**, 438-444.

8. Caughey B. and Lansbury P. T. (2003) Protofibrils, pores, fibrils, and neurodegeneration: separating the responsible protein aggregates from the innocent bystanders. *Annu. Rev. Neurosci.*, **26**, 267-298.

9. Uversky V. N. (2010) Mysterious oligomerization of the amyloidogenic proteins. *FEBS J.*, **277**, 2940-2953.

10. Mocanu M.-M., Nissen A., Eckermann K., Khlistunova I., Biernat J., Drexler D., Petrova O., Schonig K., Bujard H., Mandelkow E. *et al.* (2008) The Potential for beta-structure in the Repeat Domain of Tau Protein Determines Aggregation, Synaptic Decay, Neuronal Loss, and Coassembly with Endogenous Tau in Inducible Mouse Models of Tauopathy. *J. Neurosci.*, **28**, 737-748.

11. Eckermann K., Mocanu M.-M., Khlistunova I., Biernat J., Nissen A., Hofmann A., Schönig K., Bujard H., Haemisch A., Mandelkow E. *et al.* (2007) The beta-propensity of Tau determines aggregation and synaptic loss in inducible mouse models of tauopathy. *J. Biol. Chem.*, **282**, 31755-31765.

Downloaded from http://hmg.oxfordjournals.org/ at Universitaet Freiburg on March 21, 2013

12. Khlistunova I., Biernat J., Wang Y., Pickhardt M., von Bergen M., Gazova Z., Mandelkow E. and Mandelkow E.-M. (2006) Inducible expression of Tau repeat domain in cell models of tauopathy: aggregation is toxic to cells but can be reversed by inhibitor drugs. *J. Biol. Chem.*, **281**, 1205-1214.

13. Sydow A., Van der Jeugd A., Zheng F., Ahmed T., Balschun D., Petrova O., Drexler D., Zhou L., Rune G., Mandelkow E. *et al.* (2011) Tau-induced defects in synaptic plasticity, learning, and memory are reversible in transgenic mice after switching off the toxic tau mutant. *J. Neurosci.*, **31**, 2511-2525.

14. Santacruz K., Lewis J., Spires T., Paulson J., Kotilinek L., Ingelsson M., Guimaraes A., DeTure M., Ramsden M., McGowan E. *et al.* (2005) Tau suppression in a neurodegenerative mouse model improves memory function. *Science*, **309**, 476-481.

15. von Bergen M., Barghorn S., Li L., Marx A., Biernat J., Mandelkow E. M. and Mandelkow E. (2001) Mutations of tau protein in frontotemporal dementia promote aggregation of paired helical filaments by enhancing local beta-structure. *J. Biol. Chem.*, **276**, 48165-48174.

16. Wang Y. P., Biernat J., Pickhardt M., Mandelkow E. and Mandelkow E.-M. (2007) Stepwise proteolysis liberates tau fragments that nucleate the Alzheimer-like aggregation of full-length tau in a neuronal cell model. *Proc. Natl. Acad. Sci. USA*, **104**, 10252-10257.

17. Wang Y., Martinez-Vicente M., Kruger U., Kaushik S., Wong E., Mandelkow E. M., Cuervo A. M. and Mandelkow E. (2009) Tau fragmentation, aggregation and clearance: the dual role of lysosomal processing. *Hum. Mol. Genet.*, **18**, 4153-4170.

18. Artal-Sanz M., de Jong L. and Tavernarakis N. (2006) Caenorhabditis elegans: a versatile platform for drug discovery. *Biotechnol. J.*, **1**, 1405-1418.

19. Voisine C., Varma H., Walker N., Bates E. A., Stockwell B. R. and Hart A. C. (2007) Identification of potential therapeutic drugs for huntington's disease using Caenorhabditis elegans. *PLoS ONE*, **2**, e504.

20. Giacomotto J. and Segalat L. (2010) High-throughput screening and small animal models, where are we? *Br. J. Pharmacol.*, **160**, 204-216.

Downloaded from http://hmg.oxfordjournals.org/ at Universitaet Freiburg on March 21, 2013

21. Braungart E., Gerlach M., Riederer P., Baumeister R. and Hoener M. C. (2004) Caenorhabditis elegans MPP+ model of Parkinson's disease for high-throughput drug screenings. *Neurodegener. Dis.*, **1**, 175-183.

22. Kraemer B. C. and Schellenberg G. D. (2007) SUT-1 enables tau-induced neurotoxicity in C. elegans. *Hum. Mol. Genet.*, **16**, 1959-1971.

23. Kraemer B. C., Burgess J. K., Chen J. H., Thomas J. H. and Schellenberg G. D. (2006) Molecular pathways that influence human tau-induced pathology in Caenorhabditis elegans. *Hum. Mol. Genet.*, **15**, 1483-1496.

24. Kraemer B. C., Zhang B., Leverenz J. B., Thomas J. H., Trojanowski J. Q. and Schellenberg G. D. (2003) Neurodegeneration and defective neurotransmission in a Caenorhabditis elegans model of tauopathy. *Proc. Natl. Acad. Sci. USA*, **100**, 9980-9985.

25. Brandt R., Gergou A., Wacker I., Fath T. and Hutter H. (2009) A Caenorhabditis elegans model of tau hyperphosphorylation: induction of developmental defects by transgenic overexpression of Alzheimer's disease-like modified tau. *Neurobiol. Aging*, **30**, 22-33.

26. Guthrie C. R., Schellenberg G. D. and Kraemer B. C. (2009) SUT-2 potentiates tau-induced neurotoxicity in Caenorhabditis elegans. *Hum. Mol. Genet.*, **18**, 1825-1838.

27. Miyasaka T., Ding Z., Gengyo-Ando K., Oue M., Yamaguchi H., Mitani S. and Ihara Y. (2005) Progressive neurodegeneration in C. elegans model of tauopathy. *Neurobiol. Dis.*, **20**, 372-383.

28. Wheeler J. M., Guthrie C. R. and Kraemer B. C. (2010) The role of MSUT-2 in tau neurotoxicity: a target for neuroprotection in tauopathy? *Biochem. Soc. Trans.*, **38**, 973-976.

29. Goedert M., Baur C. P., Ahringer J., Jakes R., Hasegawa M., Spillantini M. G., Smith M. J. and Hill F. (1996) PTL-1, a microtubule-associated protein with tau-like repeats from the nematode Caenorhabditis elegans. *J. Cell. Sci.*, **109**, 2661-2672.

30. Gordon P., Hingula L., Krasny M. L., Swienckowski J. L., Pokrywka N. J. and Raley-Susman K. M. (2008) The invertebrate microtubule-associated protein PTL-1 functions in mechanosensation and development in Caenorhabditis elegans. *Dev. Genes. Evol.*, **218**, 541-551.

Downloaded from http://hmg.oxfordjournals.org/ at Universitaet Freiburg on March 21, 2013

31. Taniguchi S., Suzuki N., Masuda M., Hisanaga S., Iwatsubo T., Goedert M. and Hasegawa M. (2005) Inhibition of heparin-induced tau filament formation by phenothiazines, polyphenols, and porphyrins. *J. Biol. Chem.*, **280**, 7614-7623.

32. Wischik C. M., Edwards P. C., Lai R. Y., Roth M. and Harrington C. R. (1996) Selective inhibition of Alzheimer disease-like tau aggregation by phenothiazines. *Proc. Natl. Acad. Sci. USA*, **93**, 11213-11218.

33. Ballatore C., Brunden K. R., Piscitelli F., James M. J., Crowe A., Yao Y., Hyde E., Trojanowski J. Q., Lee V. M. and Smith A. B., 3rd (2010) Discovery of brain-penetrant, orally bioavailable aminothienopyridazine inhibitors of tau aggregation. *J. Med. Chem.*, **53**, 3739-3747.

34. Link C. D. (1995) Expression of human beta-amyloid peptide in transgenic Caenorhabditis elegans. *Proc. Natl. Acad. Sci. USA*, **92**, 9368-9372.

35. Minniti A. N., Rebolledo D. L., Grez P. M., Fadic R., Aldunate R., Volitakis I., Cherny R. A., Opazo C., Masters C., Bush A. I. *et al.* (2009) Intracellular amyloid formation in muscle cells of Abeta-transgenic Caenorhabditis elegans: determinants and physiological role in copper detoxification. *Mol. Neurodegener.*, **4**, 2.

36. Iqbal K., Alonso Adel C., Chen S., Chohan M. O., El-Akkad E., Gong C. X., Khatoon S., Li B., Liu F., Rahman A. *et al.* (2005) Tau pathology in Alzheimer disease and other tauopathies. *Biochim. Biophys. Acta*, **1739**, 198-210.

37. Kosik K. S. and Shimura H. (2005) Phosphorylated tau and the neurodegenerative foldopathies. *Biochim. Biophys. Acta*, **1739**, 298-310.

38. Augustinack J. C., Schneider A., Mandelkow E. M. and Hyman B. T. (2002) Specific tau phosphorylation sites correlate with severity of neuronal cytopathology in Alzheimer's disease. *Acta Neuropathol.*, **103**, 26-35.

39. Paquet D., Bhat R., Sydow A., Mandelkow E. M., Berg S., Hellberg S., Falting J., Distel M., Koster R. W., Schmid B. *et al.* (2009) A zebrafish model of tauopathy allows in vivo imaging of neuronal cell death and drug evaluation. *J. Clin. Invest.*, **119**, 1382-1395.

Downloaded from http://hmg.oxfordjournals.org/ at Universitaet Freiburg on March 21, 2013

40. Kosmidis S., Grammenoudi S., Papanikolopoulou K. and Skoulakis E. M. (2010) Differential effects of Tau on the integrity and function of neurons essential for learning in Drosophila. *J. Neurosci.*, **30**, 464-477.

41. Papanikolopoulou K., Kosmidis S., Grammenoudi S. and Skoulakis E. M. (2010) Phosphorylation differentiates tau-dependent neuronal toxicity and dysfunction. *Biochem. Soc. Trans.*, **38**, 981-987.

42. Ambegaokar S. S. and Jackson G. R. (2011) Functional genomic screen and network analysis reveal novel modifiers of tauopathy dissociated from tau phosphorylation. *Hum. Mol. Genet.*, **20**, 4947-4977.

43. Talmat-Amar Y., Arribat Y., Redt-Clouet C., Feuillette S., Bouge A. L., Lecourtois M. and Parmentier M. L. (2011) Important neuronal toxicity of microtubule-bound Tau in vivo in Drosophila. *Hum. Mol. Genet.*, **20**, 3738-3745.

44. Samuelson A. V., Klimczak R. R., Thompson D. B., Carr C. E. and Ruvkun G. (2007) Identification of Caenorhabditis elegans genes regulating longevity using enhanced RNAi-sensitive strains. *Cold Spring Harb. Symp. Quant. Biol.*, **72**, 489-497.

45. Lundquist E. A., Reddien P. W., Hartwieg E., Horvitz H. R. and Bargmann C. I. (2001) Three C. elegans Rac proteins and several alternative Rac regulators control axon guidance, cell migration and apoptotic cell phagocytosis. *Development*, **128**, 4475-4488.

46. Schultheis C., Brauner M., Liewald J. F. and Gottschalk A. (2011) Optogenetic analysis of GABAB receptor signaling in Caenorhabditis elegans motor neurons. *J. Neurophysiol.*, **106**, 817-827.

47. Weimer R. M., Richmond J. E., Davis W. S., Hadwiger G., Nonet M. L. and Jorgensen E. M. (2003) Defects in synaptic vesicle docking in unc-18 mutants. *Nat. Neurosci.*, **6**, 1023-1030.

48. Nonet M. L. (1999) Visualization of synaptic specializations in live C. elegans with synaptic vesicle protein-GFP fusions. *J. Neurosci. Methods*, **89**, 33-40.

49. Jin Y. (2002) Synaptogenesis: insights from worm and fly. *Curr. Opin. Neurobiol.*, **12**, 71-79.

50. Mahoney T. R., Luo S. and Nonet M. L. (2006) Analysis of synaptic transmission in Caenorhabditis elegans using an aldicarb-sensitivity assay. *Nat. Protoc.*, **1**, 1772-1777.

Downloaded from http://hmg.oxfordjournals.org/ at Universitaet Freiburg on March 21, 2013

51. Lasagna-Reeves C. A., Castillo-Carranza D. L., Sengupta U., Clos A. L., Jackson G. R. and Kayed R. (2011) Tau Oligomers Impair Memory and Induce Synaptic and Mitochondrial Dysfunction in Wild-type Mice. *Mol. Neurodegener.* , **6**, 39.

52. Schon E. A. and Przedborski S. (2011) Mitochondria: the next (neurode)generation. *Neuron*, **70**, 1033-1053.

53. Thies E. and Mandelkow E. M. (2007) Missorting of tau in neurons causes degeneration of synapses that can be rescued by the kinase MARK2/Par-1. *J. Neurosci.*, **27**, 2896-2907.

54. Klassen M. P., Wu Y. E., Maeder C. I., Nakae I., Cueva J. G., Lehrman E. K., Tada M., Gengyo-Ando K., Wang G. J., Goodman M. *et al.* (2010) An Arf-like small G protein, ARL-8, promotes the axonal transport of presynaptic cargoes by suppressing vesicle aggregation. *Neuron*, **66**, 710-723.

55. Deiana S., Harrington C. R., Wischik C. M. and Riedel G. (2009) Methylthioninium chloride reverses cognitive deficits induced by scopolamine: comparison with rivastigmine. *Psychopharmacology*, **202**, 53-65.

56. Schirmer R. H., Adler H., Pickhardt M. and Mandelkow E. (2011) "Lest we forget you - methylene blue...". *Neurobiol. Aging*, **32**, 2325.e2327-2325.e2316.

57. Pickhardt M., Larbig G., Khlistunova I., Coksezen A., Meyer B., Mandelkow E.-M., Schmidt B. and Mandelkow E. (2007) Phenylthiazolyl-hydrazide and its derivatives are potent inhibitors of tau aggregation and toxicity in vitro and in cells. *Biochemistry*, **46**, 10016-10023.

58. Earls L. R., Hacker M. L., Watson J. D. and Miller D. M., 3rd (2010) Coenzyme Q protects Caenorhabditis elegans GABA neurons from calcium-dependent degeneration. *Proc. Natl. Acad. Sci. USA*, **107**, 14460-14465.

59. Ben-Zvi A., Miller E. A. and Morimoto R. I. (2009) Collapse of proteostasis represents an early molecular event in Caenorhabditis elegans aging. *Proc. Natl. Acad. Sci. U S A*, **106**, 14914-14919.

60. David D. C., Ollikainen N., Trinidad J. C., Cary M. P., Burlingame A. L. and Kenyon C. (2010) Widespread protein aggregation as an inherent part of aging in C. elegans. *PLoS Biol.*, **8**, e1000450.

Downloaded from http://hmg.oxfordjournals.org/ at Universitaet Freiburg on March 21, 2013

61. Dillin A. and Cohen E. (2011) Ageing and protein aggregation-mediated disorders: from invertebrates to mammals. *Philos.Trans. R. Soc. B. Biol. Sci.*, **366**, 94-98.

62. Cohen E. and Dillin A. (2008) The insulin paradox: aging, proteotoxicity and neurodegeneration. *Nat. Rev. Neurosci.*, **9**, 759-767.

63. De Vos K., Grierson A., Ackerley S. and Miller C. (2008) Role of Axonal Transport in Neurodegenerative Diseases. *Annu. Rev. Neurosci.*, **31**, 151-173.

64. Ittner L. M., Fath T., Ke Y. D., Bi M., van Eersel J., Li K. M., Gunning P. and Götz J. (2008) Parkinsonism and impaired axonal transport in a mouse model of frontotemporal dementia. *Proc. Natl. Acad. Sci. USA*, **105**, 15997-16002.

65. Roy S., Zhang B., Lee V. M.-Y. and Trojanowski J. Q. (2005) Axonal transport defects: a common theme in neurodegenerative diseases. *Acta Neuropathol.*, **109**, 5-13.

66. Stamer K., Vogel R., Thies E., Mandelkow E. and Mandelkow E. M. (2002) Tau blocks traffic of organelles, neurofilaments, and APP vesicles in neurons and enhances oxidative stress. *J. Cell. Biol.*, **156**, 1051-1063.

67. Brown A. (2003) Axonal transport of membranous and nonmembranous cargoes: a unified perspective. *J. Cell. Biol.*, **160**, 817-821.

68. Mandelkow E. M., Thies E., Trinczek B., Biernat J. and Mandelkow E. (2004) MARK/PAR1 kinase is a regulator of microtubule-dependent transport in axons. *J. Cell. Biol.*, **167**, 99-110.

69. Wu Y., Wu Z., Butko P., Christen Y., Lambert M. P., Klein W. L., Link C. D. and Luo Y. (2006) Amyloid-beta-induced pathological behaviors are suppressed by Ginkgo biloba extract EGb 761 and ginkgolides in transgenic Caenorhabditis elegans. *J. Neurosci.*, **26**, 13102-13113.

70. Diomede L., Cassata G., Fiordaliso F., Salio M., Ami D., Natalello A., Doglia S. M., De Luigi A. and Salmona M. (2010) Tetracycline and its analogues protect Caenorhabditis elegans from beta amyloid-induced toxicity by targeting oligomers. *Neurobiol. Dis.*, **40**, 424-431.

71. Silva M. C., Fox S., Beam M., Thakkar H., Amaral M. D. and Morimoto R. I. (2011) A genetic screening strategy identifies novel regulators of the proteostasis network. *PLoS Genet.*, **7**, e1002438.

Downloaded from http://hmg.oxfordjournals.org/ at Universitaet Freiburg on March 21, 2013

72. Sleigh J. N., Buckingham S. D., Esmaeili B., Viswanathan M., Cuppen E., Westlund B. M. and Sattelle D. B. (2011) A novel Caenorhabditis elegans allele, smn-1(cb131), mimicking a mild form of spinal muscular atrophy, provides a convenient drug screening platform highlighting new and pre-approved compounds. *Hum. Mol. Genet.*, **20**, 245-260.

73. Medina D. X., Caccamo A. and Oddo S. (2011) Methylene blue reduces abeta levels and rescues early cognitive deficit by increasing proteasome activity. *Brain Pathol.*, **21**, 140-149.

74. Bulic B., Pickhardt M., Khlistunova I., Biernat J., Mandelkow E.-M., Mandelkow E. and Waldmann H. (2007) Rhodanine-based tau aggregation inhibitors in cell models of tauopathy. *Angew. Chem. Int. Ed. Eng.*, **46**, 9215-9219.

75. Bulic B., Pickhardt M., Mandelkow E.-M. and Mandelkow E. (2010) Tau protein and tau aggregation inhibitors. *Neuropharmacology*, **59**, 276-289.

76. Burns A. R., Wallace I. M., Wildenhain J., Tyers M., Giaever G., Bader G. D., Nislow C., Cutler S. R. and Roy P. J. (2010) A predictive model for drug bioaccumulation and bioactivity in Caenorhabditis elegans. *Nat. Chem. Biol.*, **6**, 549-557.

77. Cho J. E. and Kim J. R. (2011) Recent approaches targeting beta-amyloid for therapeutic intervention of Alzheimer's disease. *Recent Pat. CNS Drug Discov.*, **6**, 222-233.

78. Schneider A. and Mandelkow E. (2008) Tau-based treatment strategies in neurodegenerative diseases. *Neurotherapeutics*, **5**, 443-457.

79. Voisine C., Pedersen J. S. and Morimoto R. I. (2010) Chaperone networks: tipping the balance in protein folding diseases. *Neurobiol. Dis.*, **40**, 12-20.

80. Sirangelo I. and Irace G. (2010) Inhibition of aggregate formation as therapeutic target in protein misfolding diseases: effect of tetracycline and trehalose. *Expert. Opin. Ther. Targets*, **14**, 1311-1321.

81. Landau M., Sawaya M. R., Faull K. F., Laganowsky A., Jiang L., Sievers S. A., Liu J., Barrio J. R. and Eisenberg D. (2011) Towards a Pharmacophore for Amyloid. *PLoS Biol.*, **9**, e1001080.

Downloaded from http://hmg.oxfordjournals.org/ at Universitaet Freiburg on March 21, 2013

82. Sievers S. A., Karanicolas J., Chang H. W., Zhao A., Jiang L., Zirafi O., Stevens J. T., Münch J., Baker D. and Eisenberg D. (2011) Structure-based design of non-natural amino-acid inhibitors of amyloid fibril formation. *Nature*, **475**, 96-100.

83. Alavez S., Vantipalli M. C., Zucker D. J., Klang I. M. and Lithgow G. J. (2011) Amyloid-binding compounds maintain protein homeostasis during ageing and extend lifespan. *Nature*, **472**, 226-229.

84. Kayed R., Head E., Thompson J. L., McIntire T. M., Milton S. C., Cotman C. W. and Glabe C. G. (2003) Common structure of soluble amyloid oligomers implies common mechanism of pathogenesis. *Science*, **300**, 486-489.

85. Nyamsuren O., Faggionato D., Loch W., Schulze E. and Baumeister R. (2007) A mutation in CHN-1/CHIP suppresses muscle degeneration in Caenorhabditis elegans. *Dev. Biol.*, **312**, 193-202.

86. Ishihara T., Hong M., Zhang B., Nakagawa Y., Lee M. K., Trojanowski J. Q. and Lee V. M. (1999) Age-dependent emergence and progression of a tauopathy in transgenic mice overexpressing the shortest human tau isoform. *Neuron*, **24**, 751-762.

87. Sandoval G. M., Duerr J. S., Hodgkin J., Rand J. B. and Ruvkun G. (2006) A genetic interaction between the vesicular acetylcholine transporter VAChT/UNC-17 and synaptobrevin/SNB-1 in C. elegans. *Nat. Neurosci.*, **9**, 599-601.

88. Wasserman S. M., Beverly M., Bell H. W. and Sengupta P. (2011) Regulation of response properties and operating range of the AFD thermosensory neurons by cGMP signaling. *Curr. Biol.*, **21**, 353-362.

89. Gottschalk A., Almedom R. B., Schedletzky T., Anderson S. D., Yates J. R., 3rd and Schafer W. R. (2005) Identification and characterization of novel nicotinic receptor-associated proteins in Caenorhabditis elegans. *EMBO J.*, **24**, 2566-2578.

90. Wood W. B. (1988) Determination of pattern and fate in early embryos of Caenorhabditis elegans. *Dev. Biol.*, **5**, 57-78.

Downloaded from http://hmg.oxfordjournals.org/ at Universitaet Freiburg on March 21, 2013

Figure legends

Figure 1: **Panneuronal expression of pro-aggregant human Tau transgenes resulted in deposition of aggregates and locomotion defects**.

(A): Mean locomotion speed of day 1 adult animals from strains carrying independently integrated transgene arrays with pro- or anti-aggregant Tau. N2 wild type strain serves as control. Error bars denote the standard deviation (s.d.). One-way ANOVA with Tukey test was applied for comparisons (*n.s.*: non-significant).

(B): Western blot of total lysates from synchronized L4 larvae. The blots were probed with the K9JA antibody (upper panel) which recognizes the Tau repeat domain (RD) and thus detects both full length (FL) Tau and F3 fragment. Anti-actin antibody was used as loading control (lower panel). L4 larvae extracts did not show the F3 fragment but total levels of Tau expression were similar among all the different transgenic lines (normalization to actin), quantification shown in the graph below the blot. The error bars denote standard error of the mean (s.e.m.) from three repetitions of the experiment, and differences were considered non-significant ($p>0.05$) after performing one-way ANOVA.

(C): Western blot of total lysates from synchronized day 5 old adults. Both full length Tau and F3 fragment were detected with K9JA antibody. The independently integrated strains express the F3 fragment at comparable levels (normalization to actin), quantification shown in the graph below the blot. The error bars denote s.e.m. from three repetitions of the experiment, and differences were considered non-significant ($p>0.05$) after performing one-way ANOVA.

(D-F): Tau expression detected with anti-Tau K9JA antibody. Neuronal structures were stained in the anti-aggregant (E) and pro-aggregant (F) Tau transgenic strains (marked with grey arrowheads). Only background staining is observed in non-transgenic controls (D).

(G-I): Maximal Intensity Projections (MIP) of worms stained with Thioflavin-S to image Tau aggregates in the nerve ring. The strong signal in the pharynx of the animals (marked with an asterisk) derives from the transformation marker (*Pmyo-2::gfp*). Wild type strain (transformation marker only) in (G) shows only background staining, the anti-aggregant strain (H) shows very few spots, and the pro-aggregant strain in (I) shows extensive decoration with spots around the nerve ring area.

Downloaded from http://hmg.oxfordjournals.org/ at Universitaet Freiburg on March 21, 2013

(J-L): Zoom of the marked area of G-I, corresponding to the dotted rectangle region. Gray arrowheads point to individual Thioflavin-S stained Tau aggregates. Scale bars, 20 µm.

Figure 2: Sequential extraction revealed increased accumulation of insoluble Tau in the pro-aggregant strain

(A): After sequential extraction of Tau from day 1 adult transgenic *C. elegans* strains (with laboratory wild type N2 strain as control), only the pro-aggregant strain (lane 3) shows the detergent soluble (RIPA) and the detergent insoluble tau aggregates which were solubilized with 70% formic acid (FA). FL Tau V337M, but not the F3ΔK280 fragment, is phosphorylated at the KXGS motif (12E8 panel) and the S396 and S404 epitopes (PHF-1 panel). In the pro-aggregant strain, F3ΔK280 appears only in the detergent insoluble fraction (lane 3 of the FA fraction in the top panel). In contrast, F3ΔK280-PP in the anti-aggregant strain appears solely in the soluble fraction (lane 4 of the RAB fraction, top panel).

(B): Sequential extraction of Tau from day 7 adult animals. Equal amount of protein was loaded and normalized against the CK10 sample. The pro-aggregant shows approximately 2-fold soluble (RAB blot), 4-fold detergent soluble (RIPA blot) and 8-fold detergent insoluble Tau (FA blot), as quantified from 3 independent experiments (One-Way ANOVA, $*p<0.05$, $**p<0.01$, $***p<0.001$).

This data corroborate the notion that Tau displays increased aggregation when combined with the amyloidogenic F3ΔK280 fragment in the pro-aggregant strain, whereas combination with the non-amyloidogenic F3ΔK280-PP fragment, or FL Tau V337M alone, do not aggregate to such extent.

Figure 3: Morphological abnormalities accumulated in the motor neurons of the pro-aggregant Tau transgenic worms.

(A-C): Maximum Intensity Projections (MIP) of **(A):** Wild type with *Punc-25::gfp* reporter staining GABAergic motor neurons, day 1 adult. Intact ventral and dorsal cords are observed.

(B): Anti-aggregant GABAergic reporter strain, day 1 adult. No gaps are observed.

(C) Pro-aggregant GABAergic reporter strain, day 1 adult. Arrowheads point to axonal gaps along the ventral or dorsal cord. Asterisks: pharynx which expresses the transformation marker *Pmyo-2::GFP*. Scale bar, 20 µm.

Downloaded from http://hmg.oxfordjournals.org/ at Universitaet Freiburg on March 21, 2013

(D): Graph plotting the average number of gaps occurring in the neural cords of the animals as a function of time during larval development and through adulthood. Increased numbers of defects during development as well as progressive increase of gaps during adulthood were observed for the pro-aggregant strain (2-way ANOVA with Dunn's test, *****for *p<0.05,* ******for *p<0.01*, *******for *p<0.001*) Error bars: standard error of the mean (s.e.m.). 30 worms were scored per strain and per time point.

(E): Percentage of day 1 adult worms showing axonal gaps in the cholinergic motor neurons (*Punc-129::mCherry* reporter). Three times more pro-aggregant animals have axonal gaps compared to anti-aggregant animals. Error bars: s.d.

Figure 4: Defective presynaptic accumulation and organization of Synaptobrevin-1 puncta in the pro-aggregant strain.

(A-C): DIC images of the dorsal neural cord above the posterior gonadal arm of (A) wild type animals, (B) anti-aggregant and (C) pro-aggregant strains expressing the *Punc-47::snb-1::gfp* reporter. Day 1 adults are shown.

(D-F): MIP of the SNB-1::GFP fluorescent puncta (pre-synaptic termini) along the dorsal neural cord corresponding to the regions shown in the DIC pictures above. Note that for the pro-aggregation example, the SNB-1::GFP puncta are weaker and more diffuse (region between the arrowheads).

(G-I): Panel showing a compilation of 23 straightened dorsal cord segments (after binary thresholding) of day 1 adult animals expressing *Punc-47::snb-1::gfp* . **(G):** wild type, **(H):** anti-aggregant strain, **(I):** pro-aggregant strain.

(J): Scatter plot of the mean fluorescent intensity of SNB-1::GFP puncta (Arbitrary Units), as measured from the MIP images for each animal. The line denotes the mean. Kruskall-Wallis ANOVA (non-parametric) with Dunn's post hoc test was used for comparisons.

(K): Scatter plot showing the number of SNB-1::GFP puncta (synapses) per 50 µm of dorsal cord, calculated from the same images that were used for the puncta intensity quantification graph in (J). Kruskall-Wallis ANOVA with Dunn's post hoc test was used for comparisons.

Pre-synaptic SNB-1 puncta in the pro-aggregant strain often show diffuse structure and are less in numbers.

Downloaded from http://hmg.oxfordjournals.org/ at Universitaet Freiburg on March 21, 2013

Figure 5: Tau expression resulted in mild resistance against aldicarb induced paralysis but did not change levamisole sensitivity.

(A): Time course of aldicarb induced paralysis. The percentage of worms still moving on 1mM aldicarb plates after being touched with a metal wire is plotted as a function of time. The *lev-1(x21)* strain is strongly resistant to aldicarb, while the *rab-3(js49)* is mildly resistant and wild type N2 is sensitive (50). Both the pro- and anti-aggregant strains displayed slight resistance to aldicarb. Two-way ANOVA with Bonferroni correction was applied for comparisons and produced $p<0.001$ for both the pro- and anti-aggregants compared to N2 for the time points of 140, 220 and 280 min. Error bars denote s.e.m. calculated from three repetitions of the experiment (blind test).

(B): Time course of levamisole induced paralysis. The percentage of worms still moving on 0.2 mM levamisole plates after being touched with a metal wire is plotted as a function of time. The *lev-1(x21)* strain is strongly resistant to levamisole and did not paralyze. The different Tau transgenic strains paralyzed fast, at the same rate as wild type (N2), indicating levamisole sensitivity.

Figure 6: In the pro-aggregant strain mitochondria mislocalized to the proximal axonal segment of the DA9 neuron.

(A): MIP of the YFP fluorescence from the tail region of a *Pitr-1::TOM-20*$^{aa1-54}$*::yfp* wild type reporter worm, showing the distribution of labeled mitochondrial particles along the DA9 neuron. The cell body (labeled by an asterisk) is located ventrally, extending a dendrite anterior-ventrally and an axon to the anterior dorsal cord (arrowheads point to representatively labeled mitochondria). The strongly fluorescent mass in the middle is the autofluorescence of the gut. Scale bar, 10 µm.

(B): MIP of the YFP fluorescence from the tail region of a representative animal with anti-aggregant Tau. YFP-labeled mitochondria (arrowheads) are distributed along the dorsal axon, similar to wild type.

(C): MIP of the YFP fluorescence from the tail region of a pro-aggregant animal. Note the altered distribution of YFP labeled mitochondria along the DA9 neuron (the arrowheads point to mitochondria in the proximal axon, the distal segment is devoid of puncta).

Downloaded from http://hmg.oxfordjournals.org/ at Universitaet Freiburg on March 21, 2013

(D): Stacked bar diagram showing the distributions (percentage) of mitochondrial YFP particles in the proximal and distal axonal segments (the axon was arbitrarily divided in two parts of equal length for this analysis; see also Supplementary Material, Fig. S5). In wild type, around 60 % of the axonal mitochondria are located in the distal part of the axon while in the pro-aggregant strain, mitochondria cluster preferentially (60%) in the proximal part of the axon. The anti-aggregant strain shows an intermediate phenotype. 15 to 20 animals from each strain were used for quantification and error bars denote s.d. Chi-Square Test with Yates' correction was used for comparisons.

Figure 7: Mitochondrial transport was perturbed in axons of mechanosensory neurons in the pro-aggregant Tau transgenic worms.

(A-C): Representative kymographs of PLM axons from day 1 adult animals of the pro-, anti-aggregant and wild type strain derived from time-lapse imaging are shown. Vertical lines represent stationary/docked mitochondria and oblique lines (labeled by arrowheads) represent the tracks of moving mitochondria. The slope of this track is an indicator of velocity. Anterograde movements: slope declines to the right, in retrograde movements to the left. The kymograph space and time scale is shown at the bottom.

(A): wild type: two mitochondrial particles were recorded to move anterograde (arrowheads) making only short intervening pauses.

(B): anti-aggregant strain: note the oblique line in the middle which shows the track of a fast moving mitochondrial particle (arrowhead).

(C): pro-aggregant strain: Note that the two particles in motion make long pauses (oblique lines become vertical, labeled by arrowheads) and their track displacement is rather limited.

(D): Scatter plot of the mean velocities of mitochondrial particles that were manually tracked from 20 time lapse videos that were analyzed for each strain. Instantaneous velocity values that were < 10 nm/sec were not included in the calculation of the means for this plot, as these frames were classified as pause events that were separately analyzed (see next graph).

(E): Bar diagram for the quantification of pausing frequency in relation to time and distance parameter. The number of pausing events is significantly increased in the pro-aggregant strain. Error bars: s.e.m.

Downloaded from http://hmg.oxfordjournals.org/ at Universitaet Freiburg on March 21, 2013

(F): Stacked bar diagram showing the quantification of mitochondrial flux (number of mobile mitochondria/minute) and the mobile/stationary ratio (m/s ratio). No statistically significant difference was observed between the transgenics, although the ratio was slightly reduced for the pro-aggregant worms. Error bars: s.e.m.

(G): Scatter plot of the mitochondrial track displacement length that was measured for each particle from the 3 different strains. The Y axis is in log2 scale, and the line denotes the mean of each distribution. The mitochondria in the pro-aggregant worms typically covered shorter distances during comparable lengths of time lapse acquisitions (8-10 minutes for each time lapse).

In summary, the axonal transport of mitochondria in pro-aggregant worms does not run smoothly due to increased pause events and subsequently shorter track distances, although instantaneous velocities *per se* are not substantially different from those seen in the anti-aggregant worms.

Figure 8: Tau aggregation inhibitors reduced detergent insoluble Tau in the pro-aggregant Tau strain.

Sequential extraction of Tau from synchronized pro-aggregant animals after treatment with aggregation inhibitor compounds.

(A): Insoluble Tau species in the formic acid fraction (FA) decrease after Methylene Blue treatment (25 μM).

(B): Quantification of the total, soluble, detergent soluble and detergent insoluble Tau from the pro-aggregant strain after 25 μM Methylene Blue treatment. Equal amount of protein was loaded and for the quantification signal intensities were normalized against the untreated sample. The experiment was repeated three times. MB treatment leads to approximately 35% decrease in the insoluble Tau (Paired *t* test, $*p<0.05$, error bars denote s.e.m.).

(C): There is a slight decrease in the insoluble Tau extracted with formic acid (FA-blot) upon BSc3094 (25 μM) and cmp16 (100 μM) treatment but no difference after bb14 (50 μM) treatment. However, F3ΔK280 becomes only visible in the control (DMSO only).

(D): Quantification of the total, soluble, detergent soluble and detergent insoluble Tau from the pro-aggregant strain after bb14, BSc3094 and cmp16 treatment. Equal amounts of protein were loaded and for the quantification signal intensities were normalized against the untreated control (DMSO). The

Downloaded from http://hmg.oxfordjournals.org/ at Universitaet Freiburg on March 21, 2013

experiment was repeated three times. Compound bb14 leads to approximately 25% increase in the detergent soluble Tau. BSc3094 and cmp16 lead to approximately 40% and 50% decrease in the insoluble Tau respectively (One-Way ANOVA, *p<0.05, **p<0.01, ***p<0.001, error bars denote s.e.m.).

Figure 9: Tau aggregation inhibitor cmp16 partially suppressed the locomotion defect of the pro-aggregant strain and delayed the progressive accumulation of neuronal abnormalities.

(A): Mean locomotion speed of synchronized day 1 adult animals treated with either 1% DMSO (solvent control) or a series of increasing concentrations of cmp16 (in 1% DMSO). The chemical structure of the compound is depicted next to the graph, and the error bars denote s.d. Worms treated with 100 μM cmp16 showed 1.6 times faster locomotion compared to DMSO treated controls. Worms incubated with higher concentrations were not assayed (N.A.) due to compound precipitation and toxicity in the liquid cultures.

(B): Time course graph plotting the number of axonal discontinuities in the GABAergic motor nervous system of synchronized worms treated with the Tau inhibitor cmp16 or 1% DMSO control, from L1 stage until the day of scoring (day 1, day 3 and day 5 of adulthood). Cmp16 treatment reduced the accumulation of neuronal morphological abnormalities. Error bars denote s.e.m. from 3 repetitions of the experiment, with ~30 worms per group and time point. 2-way ANOVA with Bonferroni correction was implemented for comparisons (* is $p<0.05$).

Downloaded from http://hmg.oxfordjournals.org/ at Universitaet Freiburg on March 21, 2013

Abbreviations

aa	aminoacid
ANOVA	Analysis of Variance
anti-aggr.	Anti-aggregant Tau transgenic strain, expressing full length human Tau V337M plus F3ΔK280-PP fragment in the nervous system
ATPZ	Aminothienopyridazine
cmp16	Tau Inhibitor compound#16 in (33)
FTPD-17	Frontotemporal Dementia with Parkinsonism linked to chromosome 17
MB	Methylene Blue
MIP	Maximal Intensity Projection
MLS	Mitochondrial Localization Signal
NFT	Neurofibrillary Tangles
NGM	Nematode Growth Medium
pro-aggr.	Pro-aggregant Tau transgenic strain, expressing full length human Tau V337M plus F3ΔK280 fragment in the nervous system
RD	microtubule binding Repeat Domain of Tau
s.d.	Standard deviation
s.e.m.	Standard error of the mean
Tg	transgenic
ThS	Thioflavin-S

Downloaded from http://hmg.oxfordjournals.org/ at Universitaet Freiburg on March 21, 2013

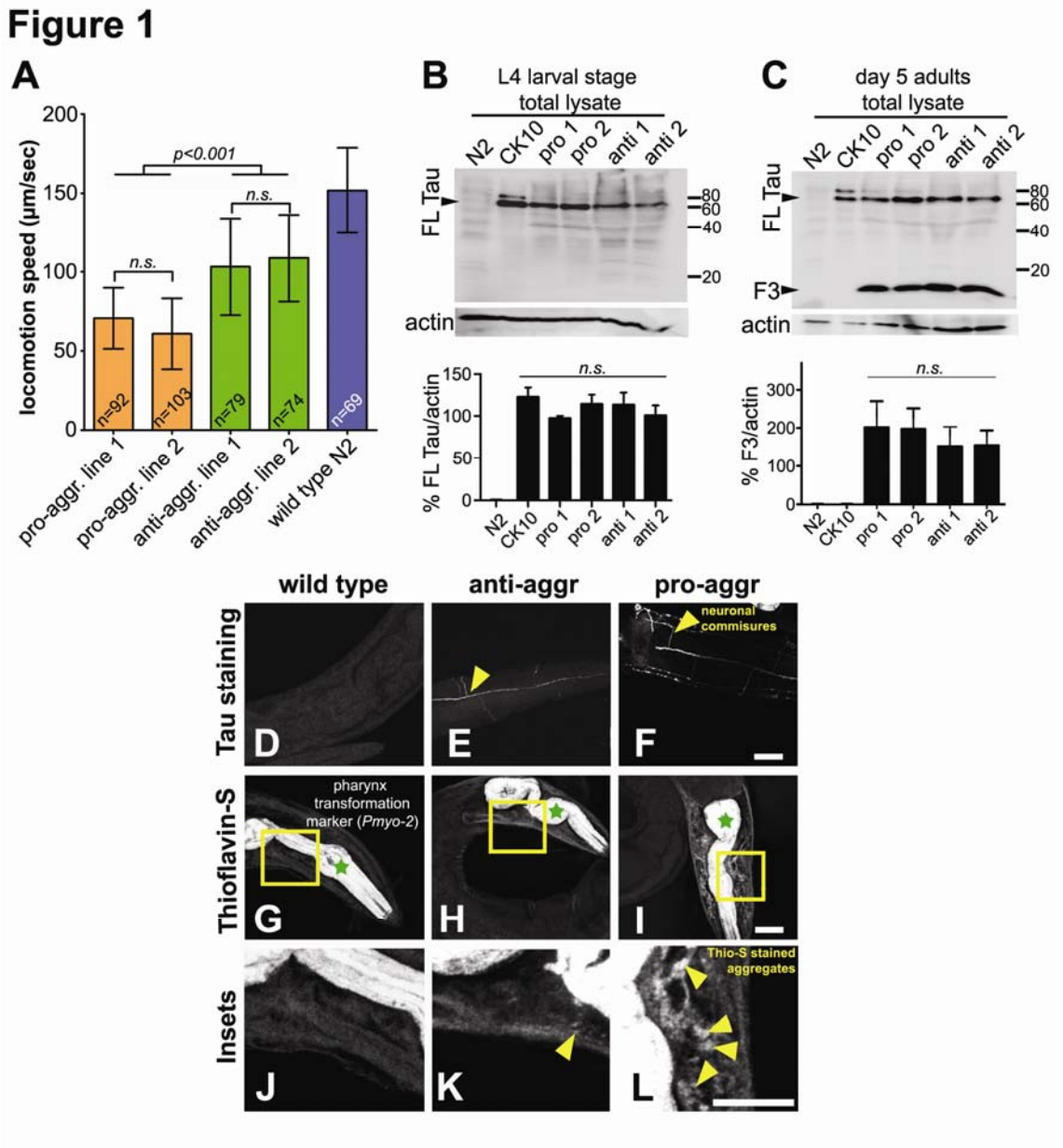

Downloaded from http://hmg.oxfordjournals.org/ at Universitaet Freiburg on March 21, 2013

Figure 2

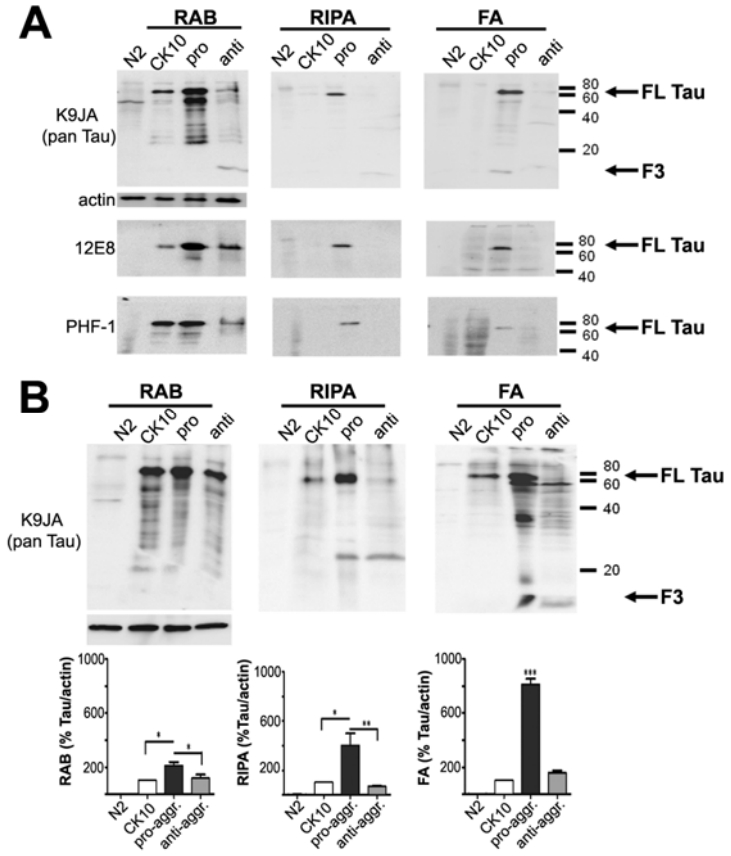

Downloaded from http://hmg.oxfordjournals.org/ at Universitaet Freiburg on March 21, 2013

Figure 3

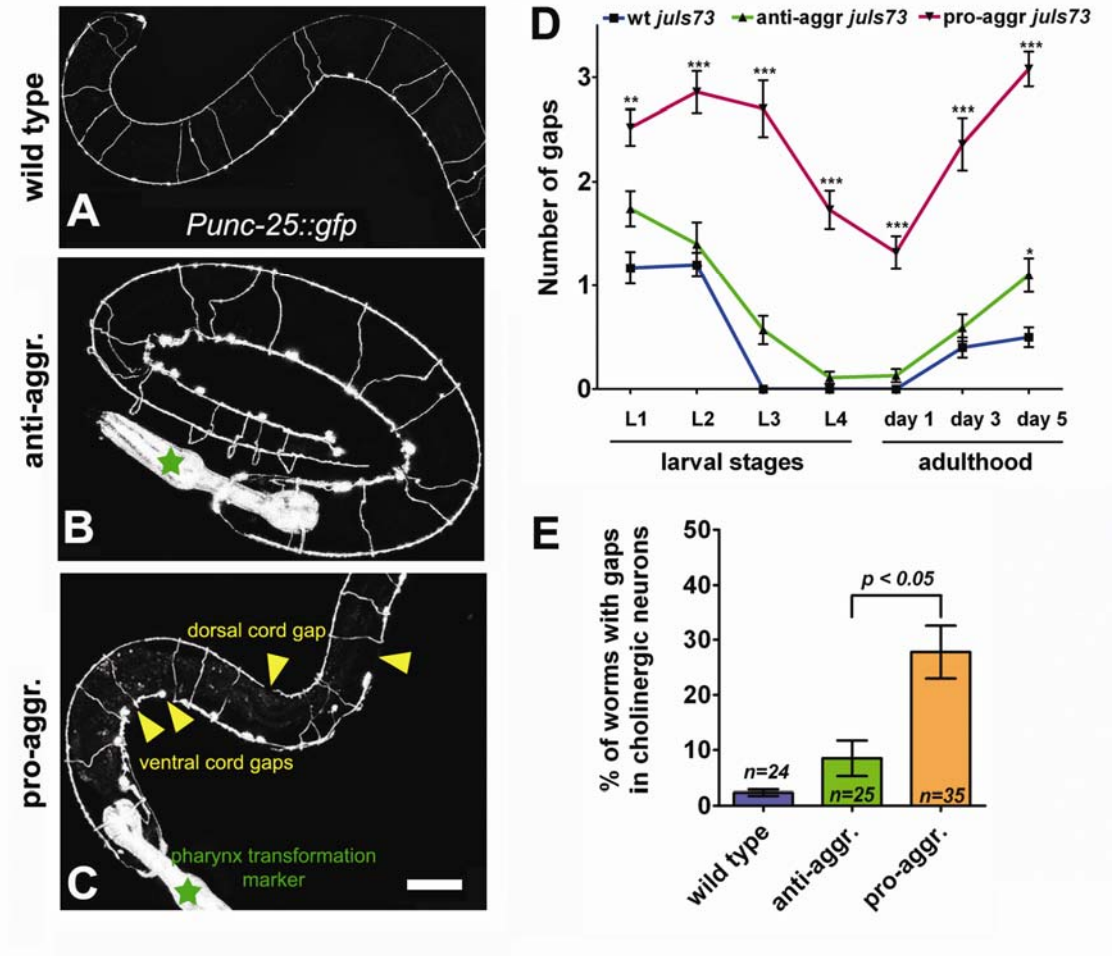

Downloaded from http://hmg.oxfordjournals.org/ at Universitaet Freiburg on March 21, 2013

Figure 4

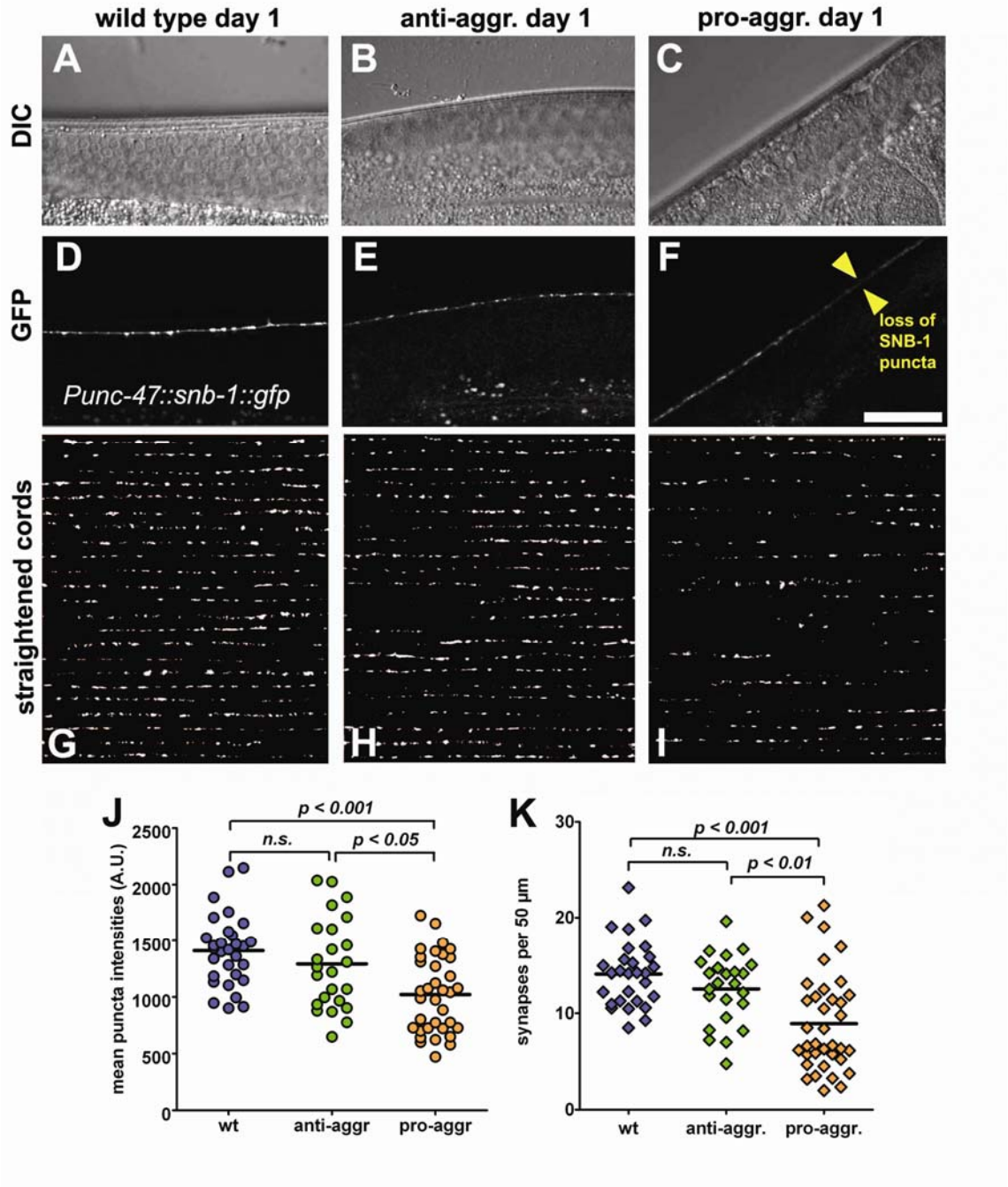

Downloaded from http://hmg.oxfordjournals.org/ at Universitaet Freiburg on March 21, 2013

Figure 5

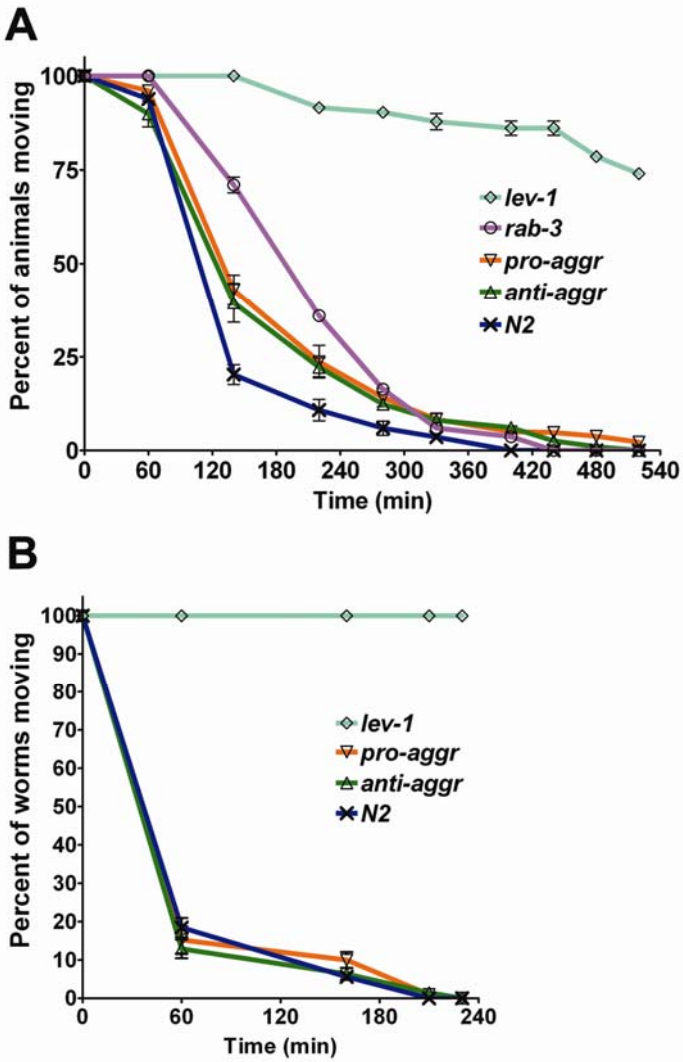

Downloaded from http://hmg.oxfordjournals.org/ at Universitaet Freiburg on March 21, 2013

Figure 6

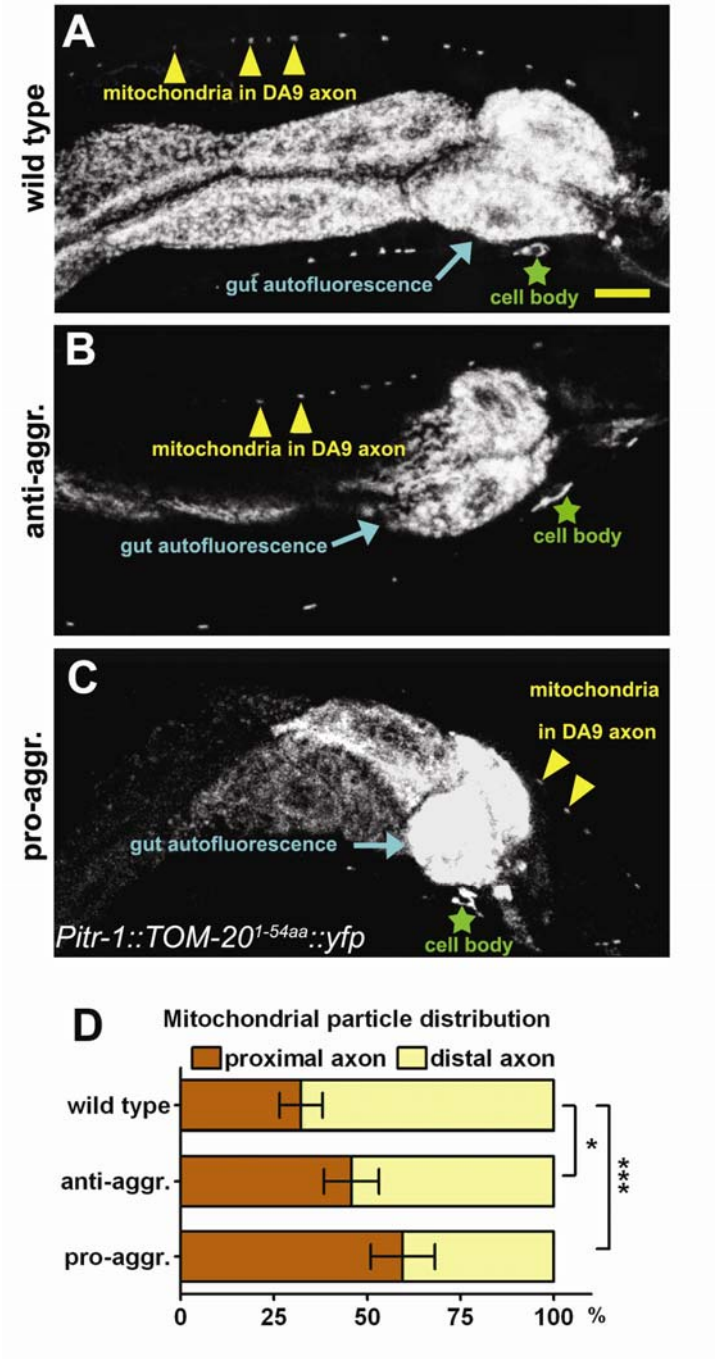

Downloaded from http://hmg.oxfordjournals.org/ at Universitaet Freiburg on March 21, 2013

Figure 7

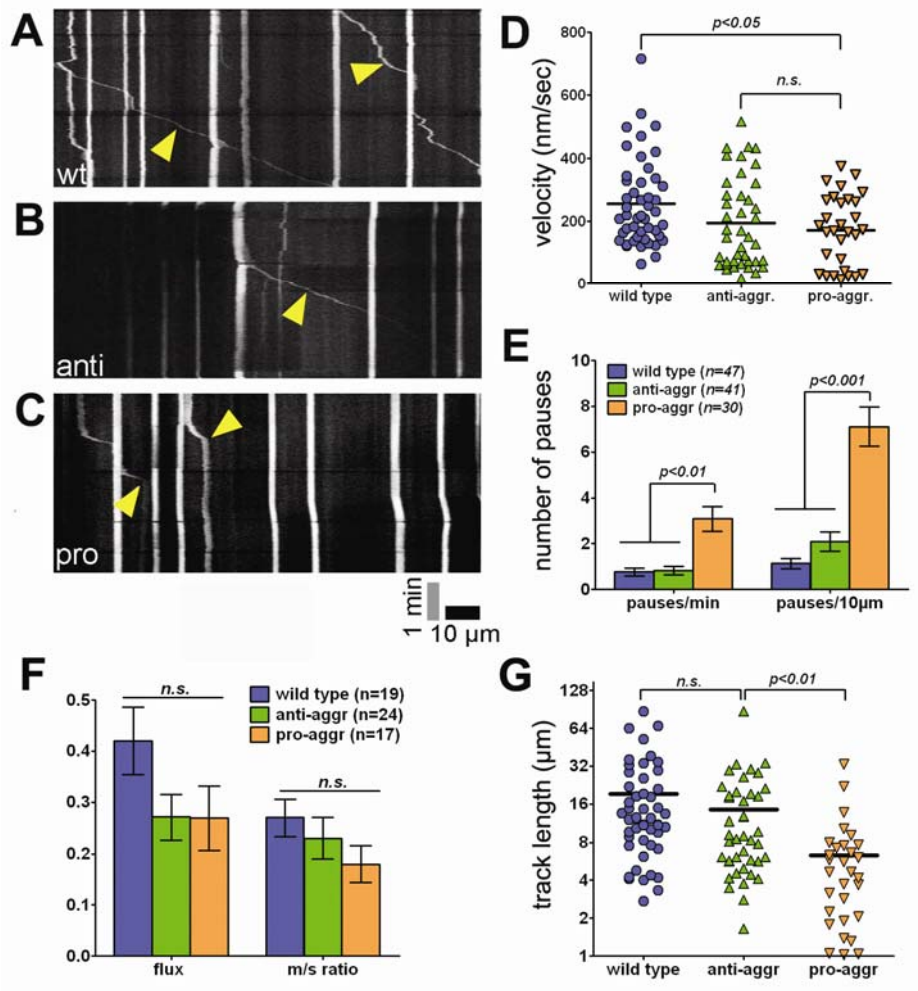

Downloaded from http://hmg.oxfordjournals.org/ at Universitaet Freiburg on March 21, 2013

Figure 8

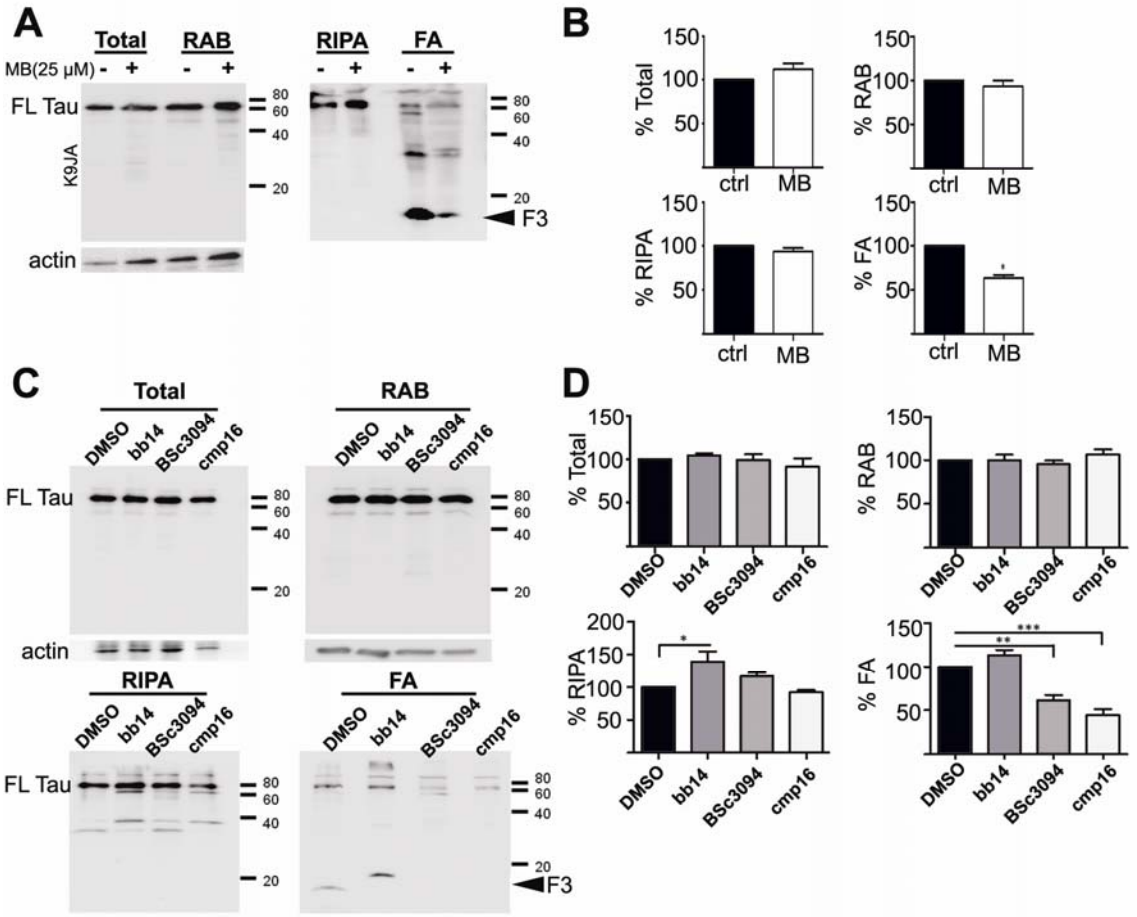

Downloaded from http://hmg.oxfordjournals.org/ at Universitaet Freiburg on March 21, 2013

Figure 9

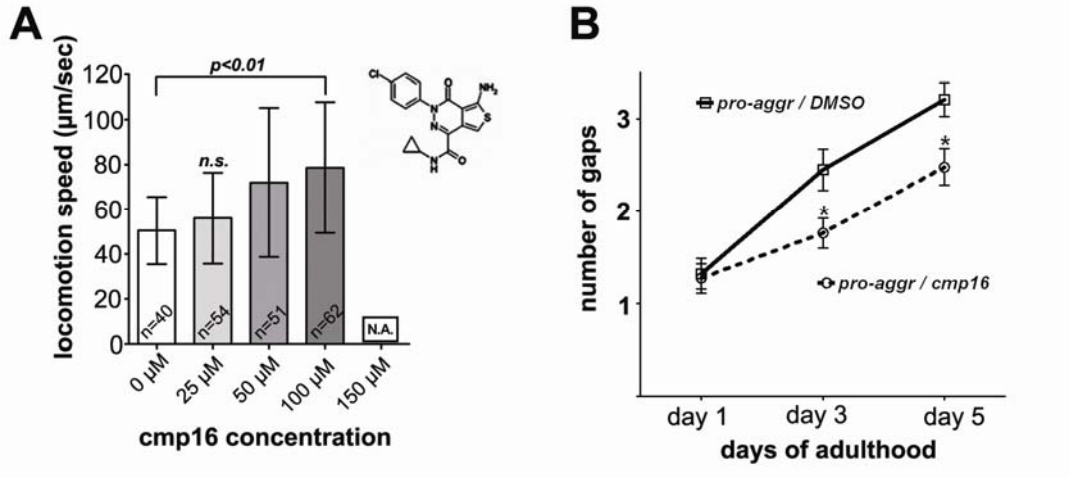

Downloaded from http://hmg.oxfordjournals.org/ at Universitaet Freiburg on March 21, 2013